

Review

Metal Oxide Semiconductor Sensors for Triethylamine Detection: Sensing Performance and Improvements

Hua Zhang , Yinghao Guo  and Fanli Meng 

College of Information Science and Engineering, Northeastern University, Shenyang 110819, China; zhanghua@ise.neu.edu.cn (H.Z.); 2100745@stu.neu.edu.cn (Y.G.)

* Correspondence: mengfanli@ise.neu.edu.cn

Abstract: Triethylamine (TEA) is an organic compound that is commonly used in industries, but its volatile, inflammable, corrosive, and toxic nature leads to explosions and tissue damage. A sensitive, accurate, and in situ monitoring of TEA is of great significance to production safety and human health. Metal oxide semiconductors (MOSs) are widely used as gas sensors for volatile organic compounds due to their high bandgap and unique microstructure. This review aims to provide insights into the further development of MOSs by generalizing existing MOSs for TEA detection and measures to improve their sensing performance. This review starts by proposing the basic gas-sensing characteristics of the sensor and two typical TEA sensing mechanisms. Then, recent developments to improve the sensing performance of TEA sensors are summarized from different aspects, such as the optimization of material morphology, the incorporation of other materials (metal elements, conducting polymers, etc.), the development of new materials (graphene, TMDs, etc.), the application of advanced fabrication devices, and the introduction of external stimulation. Finally, this review concludes with prospects for using the aforementioned methods in the fabrication of high-performance TEA gas sensors, as well as highlighting the significance and research challenges in this emerging field.



Citation: Zhang, H.; Guo, Y.; Meng, F. Metal Oxide Semiconductor Sensors for Triethylamine Detection: Sensing Performance and Improvements.

Chemosensors **2022**, *10*, 231.

<https://doi.org/10.3390/chemosensors10060231>

Academic Editor: Boris Lakard

Received: 25 May 2022

Accepted: 15 June 2022

Published: 17 June 2022

Publisher's Note: MDPI stays neutral with regard to jurisdictional claims in published maps and institutional affiliations.



Copyright: © 2022 by the authors. Licensee MDPI, Basel, Switzerland. This article is an open access article distributed under the terms and conditions of the Creative Commons Attribution (CC BY) license (<https://creativecommons.org/licenses/by/4.0/>).

Keywords: triethylamine; metal oxide semiconductor; sensing performance; morphology; new materials

1. Introduction

Emissions of noisome gases are ubiquitous in daily life and industrial production. Outdoor fuel combustion and transportation and indoor emissions from building and decorative materials, furniture, household appliances, cleaning agents, and the human body itself all produce noxious fumes. Volatile organic compounds (VOCs) are a common class of hazardous gases in the air that can have a huge negative impact on human health. As a member of VOCs, triethylamine is a colorless oily substance that is slightly soluble in water and easily dissolves in organic solvents such as ethanol; it is toxic and flammable and has a strong ammonia odor [1–3].

In many chemical synthesis processes, TEA is considered a multifunctional and efficient organocatalyst and solvent [4]. Because of its relative safety, commercial availability, and low price, it is often used in industrial production as a synthetic dye and preservative, and because of its excellent physical and chemical properties, it is also used in large quantities in chemical experiments [5]. However, when the TEA concentration is too high, it endangers our physical health by causing injuries such as skin burns and headaches as well as pulmonary edema and poisoning by accidental swallowing; its vapor can also strongly irritate the eyelids and mucous membranes [6,7]. It also has the risk of rapid burning and explosion when exposed to open fire, high temperature, and strong oxidizing agents [8,9]. Both the European Commission and the American Conference of Governmental Industrial Hygienists have recommended that the threshold concentration of TEA exposed to air be 1 ppm [10,11]. Therefore, TEA gas sensors with low detection limits that can detect quickly need to be developed.

The gas-detection methods developed so far include quartz crystal microbalance gas sensor [12], visual colorimetric detection [13], headspace gas chromatography [14], electrochemical sensors [15–17], and chemiresistive semiconductor gas sensors. The detection methods mentioned above can all detect a certain concentration of TEA, but several of them have a long detection time, high detection cost, and complicated detection operation. Therefore, the chemiresistive semiconductor sensors, which can be fast, accurate, and highly sensitive; have low detection limits; and can be manufactured in batches, have received widespread attention from scientific researchers around the world. To date, semiconductor gas sensors are mostly made of metal oxide semiconductors (MOSs), which have excellent physicochemical properties such as wide bandgap, unique microstructure [18–20], higher sensitivity to gases, and fast response time; most importantly, lower fabrication costs make them circulate in the market in large quantities. The most commonly used n-type semiconductor metal oxide materials are ZnO, SnO₂, Fe₂O₃, and MoO₃ [21], and p-type semiconductor metal materials are Co₃O₄, CuO, and NiO [22]. It is found that they all respond to TEA gas, but all have the shortcomings of low detection limit, poor stability, and high operating temperature to be solved. To improve the gas-sensing performance of TEA sensors, experimenters have been studying the uninterrupted optimization of material morphology and the compositions of different materials (MXenes, TMDs, and graphene materials) in terms of all sorts of sensing characteristics.

In the body of this review, the working principle and gas-sensing characteristics of gas sensors are introduced. More importantly, several known methods for improving the sensing performance of TEA-sensing materials are described in turn in the following sections, such as the optimization of the morphology and surface structures, combinations with other materials like metal elements and conducting polymers, the development of new materials, the application of advanced fabrication devices, and external stimulation. The conclusion and outlook are summarized at the end.

2. Gas-Sensing Characteristics

It is usually necessary to use some specific indicators to evaluate the gas-detection ability of a sensor. At present, the characteristic parameters commonly used to measure gas-sensing performance include optimal working temperature, sensitivity, selectivity, stability, repeatability, response and recovery time, and the lowest detection limits.

2.1. Optimal Working Temperature

The sensing characteristics of MOSs depend on the carrier concentration, which is relevant to the working temperature. Only at the optimum operating temperature can the sensitive materials fully stimulate the chemical activity to push the gas sensor to its maximum response. Several response curves are shown in Figure 1 [23], which often show an increase–maximum–decrease trend. When the temperature is too low, TEA molecules are inert and cannot overcome the activation energy barrier to react with the adsorbed oxygen [24]; then, as the temperature increases, the whole reaction will accelerate. However, at higher temperatures, the gas molecules get enough energy to rapidly escape from the material surface without affecting the conductivity of the sensor, resulting in the decline response [25].

At the present time, the optimal working temperature of most semiconductor sensors is high, often in hundreds of degrees Celsius, which causes huge power consumption. Developing a special gas sensor with a low operating temperature is also one of the current challenges. According to research, metals have surface redox reaction or catalytic properties, so noble doped or loaded can reduce the demand for energy input [26]. Additionally, the construction of heterojunctions can regulate carrier transport, or layered or core–shell gas-sensing materials will be more conducive to gas adsorption and desorption because of the porous structure and large specific surface area [27–29]. The above three methods are used to reduce the operating temperature of gas sensors.

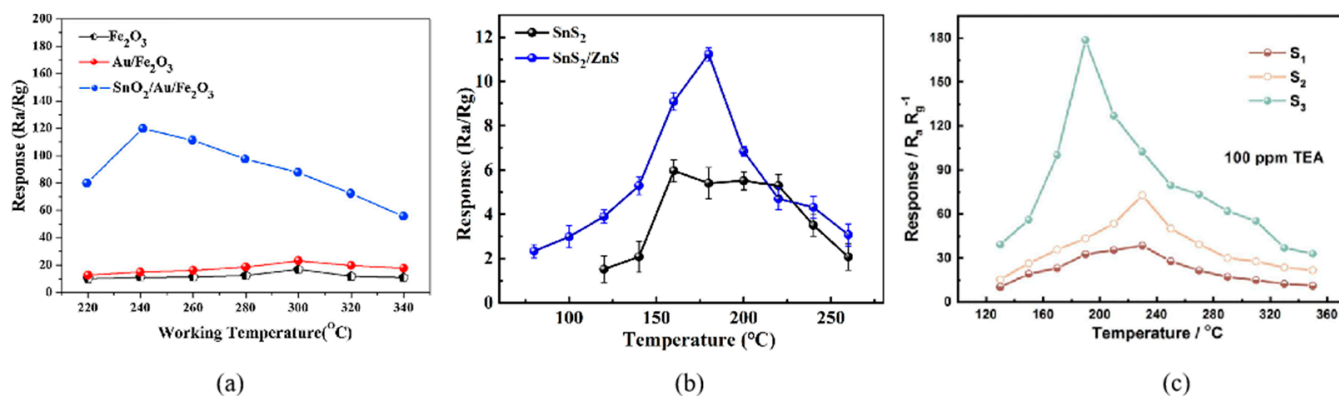


Figure 1. (a) The response curves of SnS₂ and SnS₂/ZnS to 50 ppm TEA under various working temperatures [23]; (b) The response curves of Fe₂O₃, Au/Fe₂O₃, and SnO₂/Au/Fe₂O₃ to 100 ppm TEA at different operating temperatures [30]; (c) The response curves of sample-1, -2, -3 to 100 ppm TEA at various operating temperatures [31].

2.2. Sensitivity

The sensitivity K of a gas sensor is an indicator of the responsiveness of a gas sensor to the target gas. It represents the compliance relationship between the electrical parameters of the gas sensor and the target gas concentration. There is no doubt that the greater the K value, the better the performance of the gas-sensing materials. The sensitivity K is usually expressed as $K = R_a/R_g$ (n-type semiconductor) or $K = R_g/R_a$ (p-type semiconductor) [32,33]. R_a and R_g represent the resistance of the sensor in air and in the target gas, respectively.

2.3. Selectivity

The selectivity of a gas sensor refers to its ability to recognize and measure a gas without interference from non-target gases in multigas environments [34]. In short, selectivity is the ability of a gas sensor to identify the measured gas more accurately in mixed gas. Only when the sensitivity of the target gas is several times or even tens of times higher than that of other interfering gases can a sensor be said to have good selectivity.

2.4. Stability

Stability is an important index for evaluating the property of a sensor. It refers to whether the sensor can work for a long time and still maintain or approach the initial performance within the predetermined working range [35]. Considering the practical application of gas sensors, the sensor's ability to maintain long-term stability is very necessary. Normally, the response of the prepared sensor over one or several months will be measured to ensure its stability.

2.5. Repeatability

Repeatability is defined as the ability of a semiconductor resistance sensor to restore its resistance to its original value and maintain its high sensing performance after target gas measurement. If the sensor cannot recover the resistance value in the normal gas environment, it may be that the target gas has an irreversible impact on the sensor that makes it no longer operational [36].

2.6. Response Time (τ_{res}) and Recovery Time (τ_{rec})

Response time (τ_{res}) is defined as the time required for the resistance value of a sensor in the air to reach 90% of the resistance value in the measured gas. Similarly, recovery time (τ_{rec}) is specified as the time required to recover to 90% of the resistance value in the air after removing the target gas [37]. The preparation of sensors that can quickly detect TEA gas is also one of the directions that people are vigorously studying.

2.7. The Lowest Detection Limits

The lowest detection limit is one of the major indexes pursued by many TEA sensors. It refers to the minimum gas concentration that can make the sensor respond under certain conditions, that is, the minimum detection concentration. High-performance sensors with low detection limits can often detect parts from per million (ppm) or even lower to parts per billion (ppb) [38]. This makes it possible to capture mixed harmful gases in the air much earlier when gases leaks.

A comparison of the performance of several TEA sensors is given in Table 1.

Table 1. The sensing characteristics of several typical triethylamine sensors.

Nanomaterial Shapes	τ_{res}/τ_{rec} (s)	T (°C)	Conc. (ppm)	Lim. (ppm)	Res.	Ref.
SnS ₂ /ZnS microspheres	2/8	180	50	-	11.21	[23]
ZIF-67/PBA arrays	5/182	180	100	-	11.7	[24]
ZnFe ₂ O ₄ -ZnO mesoporous	0.9/23	240	50	-	21.23	[25]
Au-PdO Modified Cu-Doped K ₂ W ₄ O ₁₃ Nanowires	17/27	120	10	1	282	[26]
mesoporous ZnO/Co ₃ O ₄ nanosheets	17/25	240	50	0.087	67.8	[27]
COFs@SnO ₂ @carbon nanospheres	7/5	RT	2	0.2	95.1	[28]
ZnO/SnO ₂ micro-camellia	27/12	100	100	1	780	[29]
yolk-shell SnO ₂ /Au/Fe ₂ O ₃ nanoboxes	7/10	240	100	0.05	126.84	[30]
Zn ₂ SnO ₄ /ZnSnO ₃	19/37	190	100	0.5	179.7	[31]
ZnO/Co ₃ O ₄ nanomeshes	30/55	100	5	-	3.2	[32]

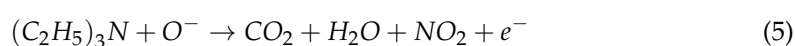
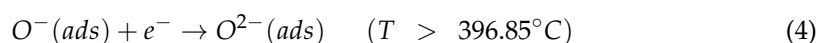
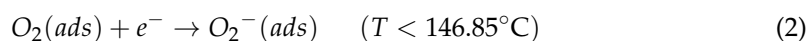
Note: τ_{res} and τ_{rec} represent response times and recovery times, respectively. T and Conc. indicate the optimal working temperature and detection concentration, respectively. Lim. is the abbreviation of the lowest detection limit. And Res. and Ref. represent response and reference, respectively. RT represents room temperature.

3. Triethylamine Gas Sensing Mechanism

To date, scientists have used various ways to explain the gas-sensing mechanism of semiconductor sensors. Several widely used theories are electron depletion layer theory, hole accumulation layer theory, bulk resistance control mechanism, and gas diffusion control mechanism.

3.1. Electron Depletion Layer (EDL) Theory

For n-type semiconductors, the gas-sensing mechanism is more often explained using electron depletion layer theory. As an n-type semiconductor, the main carriers are negatively charged electrons [39]. When the sensor is in an air environment, oxygen molecules are adsorbed on the material surface, and the material traps its free electrons in the conduction band, forming the surface adsorption of O²⁻, O⁻ and O₂⁻, described by Equations (1)–(4) [40]. The result is the formation of an electron depletion layer on the sensor surface, which leads to an increase in resistance. At this point, TEA gas is passed and will undergo a redox reaction with the adsorbed oxygen on the material surface, while the captured electrons will be released back into the conduction band, the process of which is described by Equation (5) [40]. This process will significantly reduce the Schottky barrier height and decrease the depletion layer thickness, leading to lower resistance. An typical image of the mechanism is shown in Figure 2 [41].



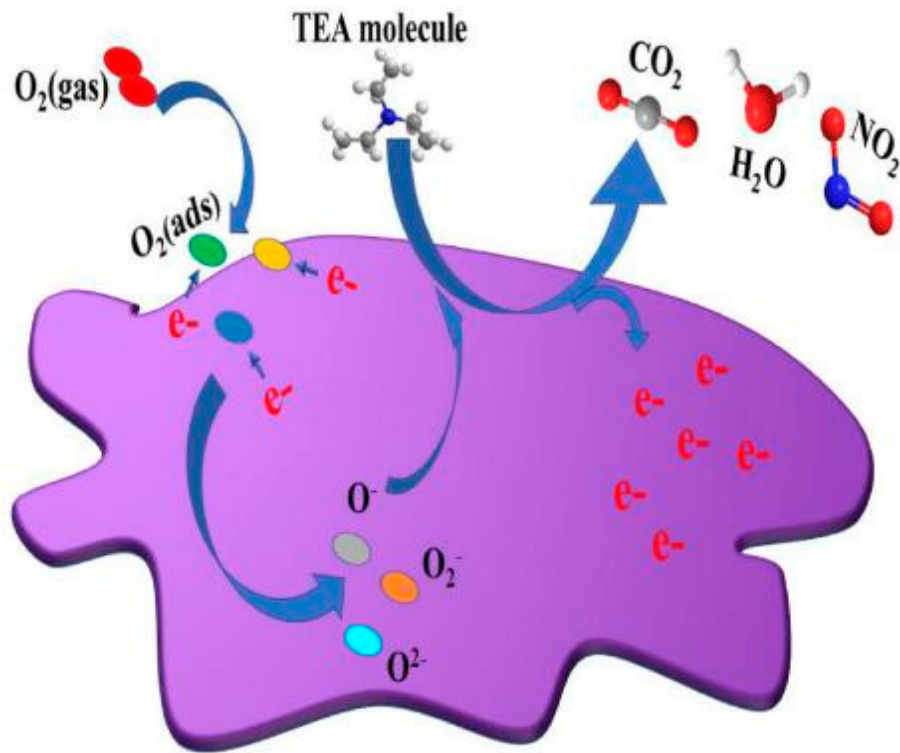
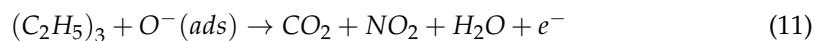
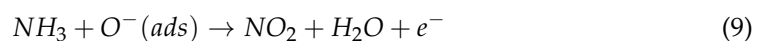


Figure 2. One typical n-type gas-sensing mechanism for an SnWO₄ sensor exposed to air and TEA gas [41].

3.2. Hole Accumulation Layer (HAL) Theory

For p-type semiconductors, the gas-sensing mechanism is more often explained using hole accumulation layer theory. As a p-type semiconductor, the main carriers are positively charged holes. In the air, oxygen molecules come in contact with the material and draw electrons out of the conduction band; they are then adsorbed on the surface to form chemisorbed oxygen (O^{2-} , O^-) [42]. The loss of electrons results in the formation of HAL on the surface and a concomitant decrease in the resistance of the sensor. The process is represented by Equations (6) and (7) [43]. When the sensor is exposed to TEA gas, the gas molecules adsorbed on the material surface undergo a chemical reaction and decompose into ammonia and ethylene, and the chemisorbed oxygen oxidizes the ammonia and ethylene to nitrogen dioxide, carbon dioxide, and water. Then, the free electrons return to the material surface, the thickness of HAL decreases, and the resistance of the sensor gradually returns to the original value. The process is represented by Equations (8)–(11) [43]. An example image of the mechanism is shown in Figure 3.



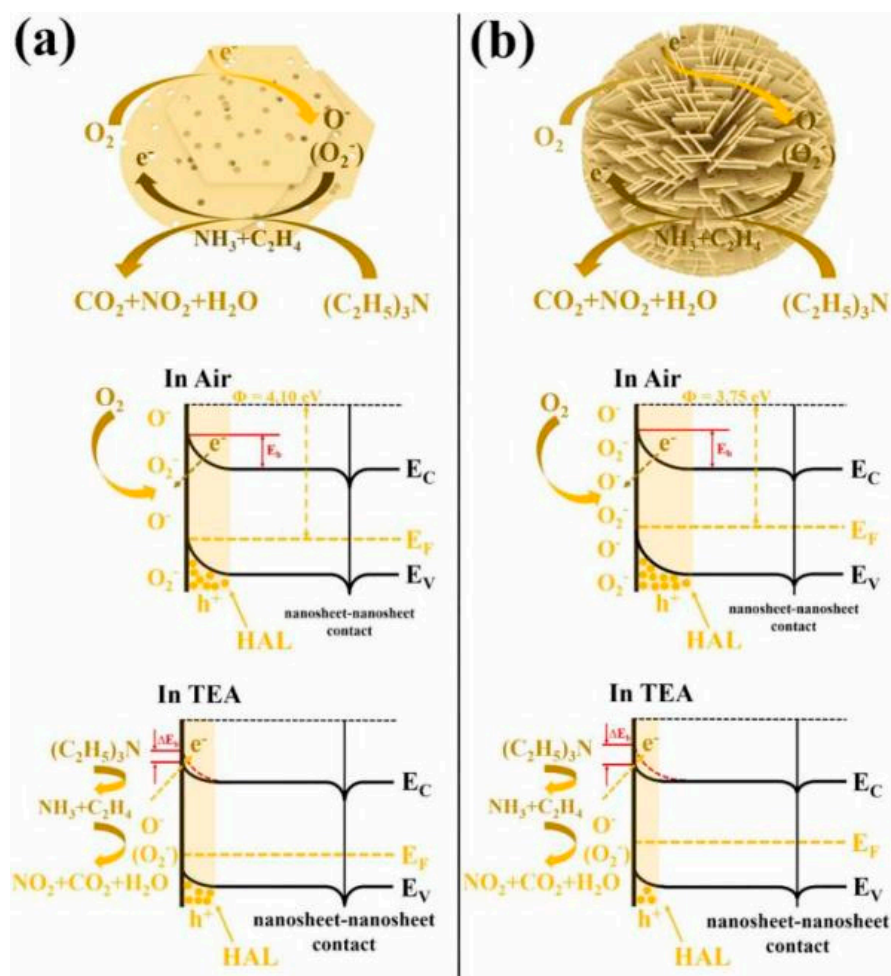


Figure 3. Typical p-type gas-sensing mechanisms for (a) Co_3O_4 sheet-300 and (b) Co_3O_4 sphere-300 [43].

4. Optimizing the Material Shape and Surface Structure

As is known to all, the gas-sensing performance of nanomaterials is partly determined by their ability to convert oxygen in the air into lattice oxygen. The stronger the conversion ability, the better the gas-sensing performance will be [44]. Obviously, the conversion ability is affected by the morphological structure of nanomaterials because the larger the specific surface area and porosity of the nanomaterials, the more active sites will adsorb oxygen, and the stronger their ability to adsorb oxygen. Researchers have prepared such nanomaterials as zero-dimensional (nanocrystals [45], nanoparticles [46], quantum dots), one-dimensional (nanorods [47,48], nanowires [49], nanofibers), two-dimensional (nanosheets [50], nanofilms), three-dimensional (nanoflowers [51], nanospheres [51], nanoflowers [52]), and other nanomaterials by hydrothermal method, solvothermal method, and sol-gel method. In addition, nanocrystals also have complex surface structures, with clear shapes and exposed crystal surfaces [53]. Semiconductor nanocrystals usually have different surface structures on the atomic scale and exhibit different physical and chemical properties. It can be inferred that adjusting the different exposed crystal planes of nanomaterials also plays a key role in the sensing performance of TEA.

4.1. Zero-Dimensional (0D) Nanomaterials

Low-dimensional nanomaterials such as 0D nanoparticles and nanocrystals are the earlier nanomaterials prepared for gas sensors [54,55]. Because of their small specific surface area and low porosity compared with other dimensional nanomaterials, they often need

some ways to improve their gas-sensing characteristics [56], although some 0D materials do have good sensing performance.

Yu et al. [57] synthesized hierarchical hollow GaFeO_3 by a kind of solvothermal method and a subsequent annealing strategy. They obtained $\text{Fe}_4[\text{Fe}(\text{CN})_6]_3$ MOF precursors through a facile hydrothermal process and then used Ga^{3+} as the modifier to modify the precursors. The hollow porous nanocube microstructure was vividly depicted by TEM, SEM, and XRD in Figure 4. They found that the microsized morphologies and hollow interior structures of GaFeO_3 microcubes can be feasibly modulated by controlling the thermolysis temperatures. The ultrasmall GaFeO_3 nanostructure exhibited rapid response times (9 s), good selectivity, and excellent stability.

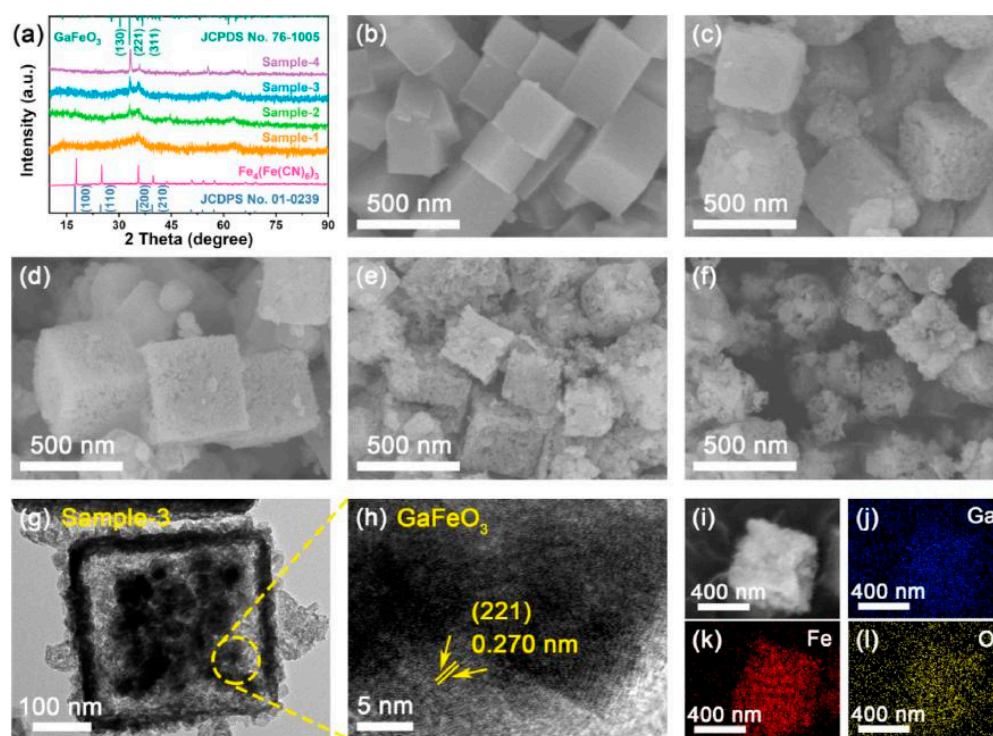


Figure 4. (a) From bottom to top, the simulated and experimental XRD patterns of $\text{Fe}_4[\text{Fe}(\text{CN})_6]_3$ MOFs (JCPDS No. 01–0239), the experimental XRD patterns of Samples-1, -2, -3, -4, and the simulated XRD pattern of GaFeO_3 phase (JCPDS No. 76–1005). The FE-SEM images of (b) $\text{Fe}_4[\text{Fe}(\text{CN})_6]_3$ MOF precursors and (c–f) porous GaFeO_3 microcubes of Samples-1, -2, -3 and -4 obtained at 400, 450, 500, and 550 °C, respectively. (g) TEM and (h) HRTEM images of Sample-3 obtained at 500 °C. (i) The selected SEM image of Sample-3 and the corresponding elemental mapping images of (j) Ga, (k) Fe, and (l) O, respectively [57].

Meng et al. [58] successfully synthesized SnO_2 nanoparticles with abundant oxygen vacancies (OVs) by a combined hydrothermal route and ice-water bath stirring method. The sensors based on this material reveal excellent selectivity, ppb level detection limit, and long-term stability. The outstanding sensing characteristics of the sensor could be attributed to the abundant OVs, improving the O_2 adsorptivity and enhancing electron transfer. Du et al. [59] synthesized SnO_2 quantum dots with controllable size by changing the amounts of hydrazine in the hydrothermal process. The experimental results show that the smaller the SnO_2 quantum dot material, the better the sensing performance for VOC gases. More critically, it has a faster response time and a lower detection limit for TEA than other VOC gases.

4.2. One-Dimensional (1D) Nanomaterials

Hierarchical materials with 1D structures can be used to design adjustable surface-active regions to obtain more reactive sites, boost electron transmission efficiency, and optimize electron transmission channels [60–62]. Moreover, 1D hierarchical structures can inhibit aggregation, resulting in significantly improved gas dispersion and transfer [63].

Lv et al. [64] successfully fabricated well-crystallized ZnO nanorods using a simple solution route with dodecyl benzene sulfonic acid sodium salt as a modifying agent. The experiment results reveal that this material has a low working temperature (150 °C), excellent selectivity, and superior sensitivity to ppm level TEA. In another study, Liu et al. [65] fabricated ultralong NiO nanowires assembled with NiO nanocrystals by adjusting the hydrothermal reaction temperature and time to enhance the gas-sensing properties. The TEM images of the structural representations of the material are shown in Figure 5, and typical transient response curves of several powders of NiO are exhibited in Figure 6. The curves indicate the improvement in gas sensing of ultralong NiO nanowire compared with the other two nanomaterials.

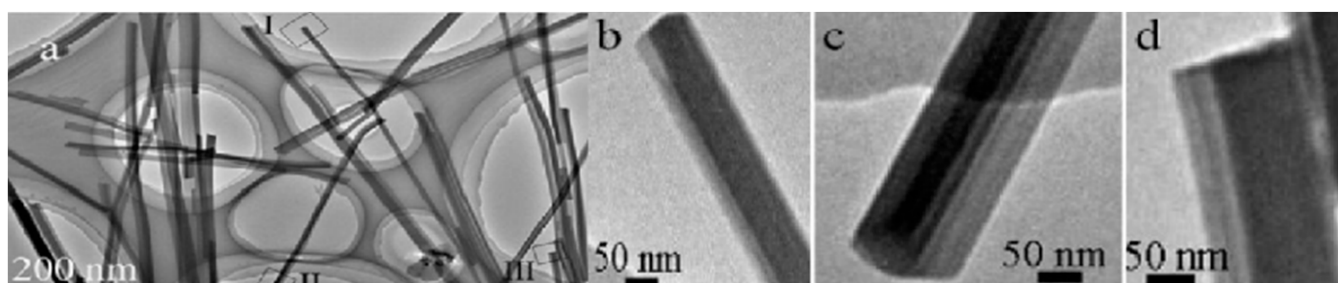


Figure 5. (a) The typical TEM images of the $\text{NiC}_2\text{O}_4 \cdot 2\text{H}_2\text{O}$ precursors prepared at 220 °C for 12 h. (b–d) TEM images at high magnification from rectangles I–III in [65].

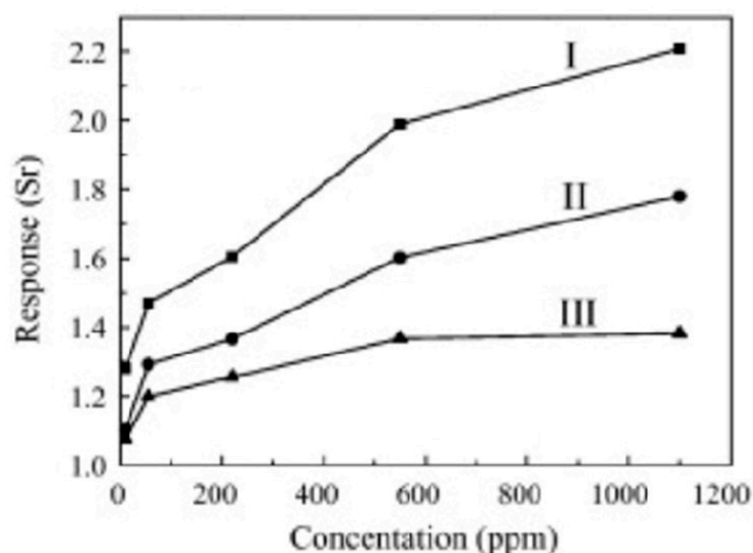


Figure 6. The response of the sensors is based on (I) the ultra-long nanowires, (II) nanowires, and (III) powders of NiO to triethylamine of different concentrations [65].

Zou et al. [66] reported a hollow SnO_2 microfiber that was prepared via a unique sustainable biomass conversion strategy for highly efficient TEA detection. The authors established that the unique structure efficiently immobilized Sn^{2+} cations during the subsequent calcination process to synthesize the hollow SnO_2 microfiber. The excellent TEA gas property in turn contributed to the synergism of the 1D carbon morphology and the porous hollow structure.

4.3. Two-Dimensional (2D) Nanomaterials

Mesoporous or layered 2D nanomaterials composed of nanoparticles often have large specific surface area and porosity, which also gives them good sensitivity, long-term cycle stability, and excellent selectivity, which is more conducive to the detection of TEA [67]. Researchers today are still focusing on research and development related to different 2D nanostructures to improve gas-sensing performance.

Zhang et al. [68] used polystyrene-polyacrylic acid ZIF-8 as the collaborative template by calcination precursor for 2 h to obtain mesoporous ZnO nanosheets. The team completely characterized the morphology as well as the microstructure and specifically tested the gas properties for TEA. The test results show that the high response to 50 ppm TEA can reach 43.771 at 268 °C. Meanwhile, the low detection limit (1 ppm) and rapid response/recovery are also advantages of the material. In one recent report, Liu et al. [69] designed 2D ultrathin SnO₂ nanofilms for manufacturing low-temperature TEA gas sensors. They studied the effect of calcination temperature on crystal crystallization and found that with the increase in temperature, the crystal size decreased, and the uniformity and density of the surface particles gradually increases. Furthermore, the decrease in crystallinity combined with the increase in interfacial defects led to the suppression of grain boundary migration and an increase in the energy barrier for grain growth.

4.4. Three-Dimensional (3D) Nanomaterials

There are now a variety of 3D porous core-shell, layered, microsphere, and other nanostructures assembled by low-dimensional nanomaterials with greatly increased specific surface areas and active sites that can promote the adsorption and transmission of gas molecules [70]. The increased specific surface areas and pore diameters of 3D porous hollow structures also avoid agglomeration [71,72].

Wang et al. [73] prepared a 3D porous ZnO foam structure through a simple solvothermal method by dissolving Zn(NO₃)₂·6H₂O solid in ethylene glycol solution and calcining the precipitate at 350 and 450. The sample obtained at 350 °C showed an excellent response to low-concentration TEA. One type of WO₃ hollow microsphere for fast TEA gas sensing was successfully prepared by Zhai et al. [74]. They used a simple low-temperature solvothermal strategy followed by an annealing process in atmospheres. The fabricated WO₃ hollow microspheres material shows excellent selectivity and fast response time to 50 ppm TEA at 220 °C. The response is almost greater than that for all of the previously reported TEA sensors. In the SEM images shown in Figure 7, we can clearly see the microsphere structure of the prepared material. Its large specific surface area and hollow structure play a key role in improving its response speed. Sui et al. [75] constructed three-dimensional novel flower-like α-MoO₃ with hierarchical structure via a facile solvothermal route without any surfactant or template and performed subsequent calcination at 400 °C in the air for 2 h. The experimental results present that at the working temperature of 250 °C, this material to 100 ppm TEA not only attains a high response (416) but a low detection limit (0.5 ppm). However, the long recovery time is also a big problem to be solved.

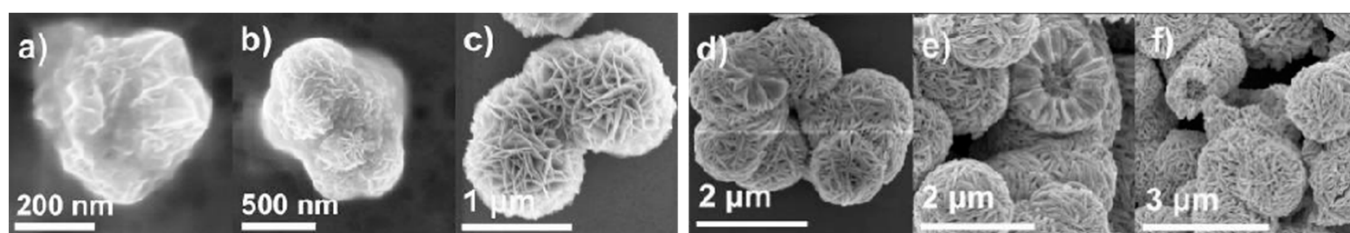


Figure 7. (a–e) SEM images of the hollow microsphere samples prepared after 10 min; 15 min; 30 min; 2 h; and 6 h hydrothermal reaction time. (f) SEM image of the WO₃ hollow microspheres after annealing [74].

4.5. Exposed Crystal Plane

Lattice is the regular arrangement of atoms in the crystal. In the process of spontaneous growth, crystals can develop polyhedral shapes composed of planes with different orientations [76]. The planes in these polyhedral shapes are called crystal faces. Crystal will produce two different situations: anisotropic and isotropic. The anisotropy of crystals means that the periodicity and density of the arrangement of protons are different along with different directions of the lattice, resulting in different physical and chemical properties of crystals in different directions. The opposite is isotropy, that is, the physical and chemical properties of crystals in different directions are the same. The crystals often show anisotropy, so they often show different gas-sensing characteristics when exposed to different crystal planes [77].

There are few reports on the effect of exposed crystal on TEA gas sensing; however, Xu et al. [78] prepared SnO₂ nanorods with {200} crystal faces and successfully made normal SnO₂ nanorods with outstanding TEA selectivity. Xiang et al. [79] make a profound study of the TEA-sensing characteristics of nonpolar (11–20) and polar (0001) GaN thin films. The results show that Mn atoms at (111) surface show remarkably improved sensing properties, which allows the active unsaturated Mn atoms to adsorb oxygen, creating electrons and catalyzing the gas-sensing reaction.

In Table 2, the reaction of nanomaterials with different morphology and exposed crystal surface to TEA is sorted out.

Table 2. TEA-sensing properties of different gas-sensing material shapes.

	Nanomaterial Shapes	τ_{res}/τ_{rec} (s)	T (°C)	Conc. (ppm)	Lim. (ppm)	Res.	Ref.
0D	hollow GaFeO ₃ microcubes	9/49	200	200	-	7.4	[57]
	SnO ₂ nanoparticles	163/163	260	100	0.001348	430.65	[58]
	SnO ₂ quantum dots	1/47	240	100	1	153	[59]
1D	ZnO nanorods	15/15	150	1	0.1	39	[64]
	NiO nanowires	-	350	9	2	3.5	[65]
	Hollow SnO ₂ Microfiber	14/12	270	100	2	49.5	[66]
2D	ZnO nanosheet	7/21	268	50	1	43.771	[68]
	SnO ₂ nanofilms	-	150	100	-	19.2	[69]
3D	porous ZnO foam	1/1	350	100	<5	79.5	[73]
	WO ₃ hollow microspheres	1.5/22	220	50	-	16	[74]
	flower-like α -MoO ₃	3 s/1283	250	100	0.5	416	[75]
crystal face	SnO ₂ nanorods {200} crystal faced	6 s/465	120	50	-	64	[78]
	polar (0001) GaN thin films	7.9 s/20.7	480	200	0.2	5.23	[79]

5. Combinations of Different Materials

Although the metal oxide of a single metal has a certain response to VOCs, most of the materials have a high intrinsic value band, leading to weak gas adsorption capacity and resulting in low sensitivity, poor selectivity, and insufficient response speed. In the process of continuously improving the performance of the sensor, researchers found that combinations of different materials can often increase the adsorption sites and reduce the reaction energy consumption [80]. Several material combination methods for improving the sensing ability will be introduced below.

5.1. Effect of Metal Elements and Non-Metallic Elements

Among the sea of methods for enhancing the gas-sensing characteristics of gas-sensing materials, the use of metal or nonmetallic elements to dope and modify the target materials is the most convenient and popular [81]. Both the catalysis of metal materials and the

electronic properties of nonmetallic materials can reduce the adsorption energy of gas [82], and the formation of defects on the surface and modification of the electronic structure can also play a role in improving sensing properties [83]. The action of metal elements can be simply divided into two categories, doped and surface decoration, and the action of nonmetallic elements can be roughly divided into doped and conductive polymer composite modification.

5.1.1. Role of Transition Metals, Noble Metals, and Rare Earth Elements

Through a large number of studies, it is found that noble metals and transition metals have strong catalytic properties and can replace the metal ion sites in the original materials to form more oxygen vacancies and surface adsorption sites, so as to improve the adsorption performance of gas. Therefore, transition metals such as Fe, Cr, Ni, Co, Ce, Cu, and noble metals such as Ag, Au, Pt, and Pd have been utilized as dopants into nanostructured [84,85]. In addition, rare earth elements such as Y, Sc, La, Ce, Ho, and Gd with unique electronic shells as dopants can cause lattice deformation and defects, increasing the number of oxygen vacancies and improving the gas adsorption capacity [86].

Liu et al. [87] loaded Pt nanoparticles on InO₃ novel hierarchical ZnO microspheres via a two-step hydrothermal method. They not only compared the TEA gas-sensing performance of the prepared Pt-ZnO nanospheres with that of commercial ZnO but also discussed the role of Pt decoration in enhancing the gas-sensing properties. Figure 8 depicts that the responses of the self-made ZnO nanospheres mixed with Pt at 200 °C are much higher than those of commercial ZnO and the self-made nanospheres without Pt. Zhu et al. [88] dropped different holmium ions concentrations of 0 at.%, 0.11 at.%, 0.45 at.%, and 0.53 at.% in SnO₂ nanoparticles (NPs) via gas–liquid phase chemical deposition following annealing. Figure 9 the presents the TEM images of the process, showing that Ho particles are already dropped in SnO₂. Meanwhile, Figure 10 reveals the brief enhancement of its TEA gas-sensing properties.

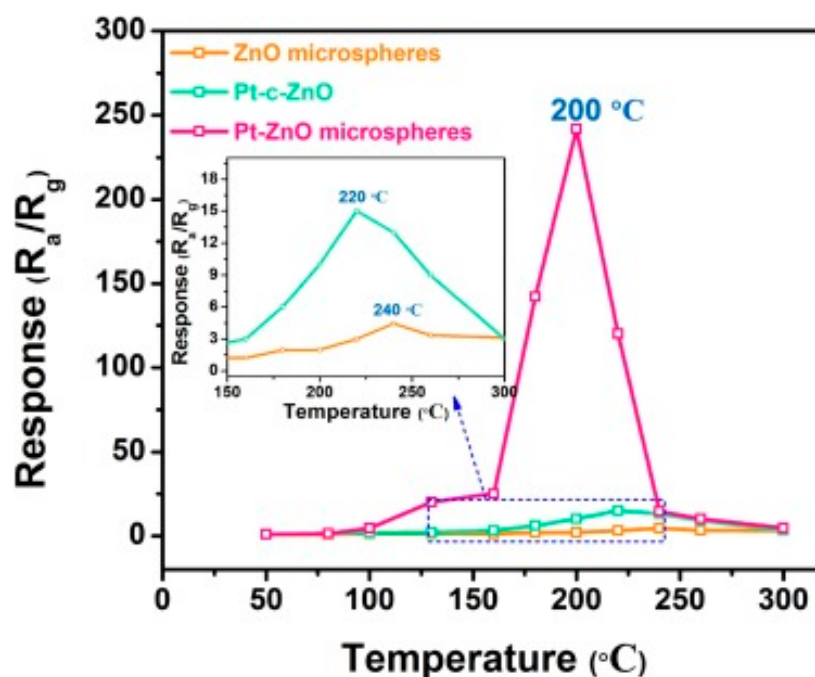


Figure 8. The response curves of the ZnO, Pt-c-ZnO, and Pt-ZnO microspheres to 100 ppm TEA at various temperatures [87].

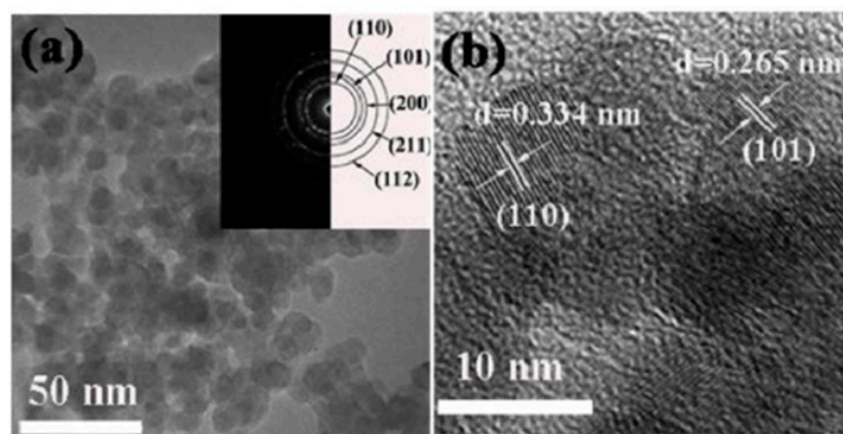


Figure 9. (a) TEM images of 0.45 at% SnO₂: Ho³⁺ nanoparticles. The inset is the SAED image of 0.45 at% SnO₂: Ho³⁺ nanoparticles. (b) The HRTEM image of 0.45 at% SnO₂: Ho³⁺ nanoparticles [88].

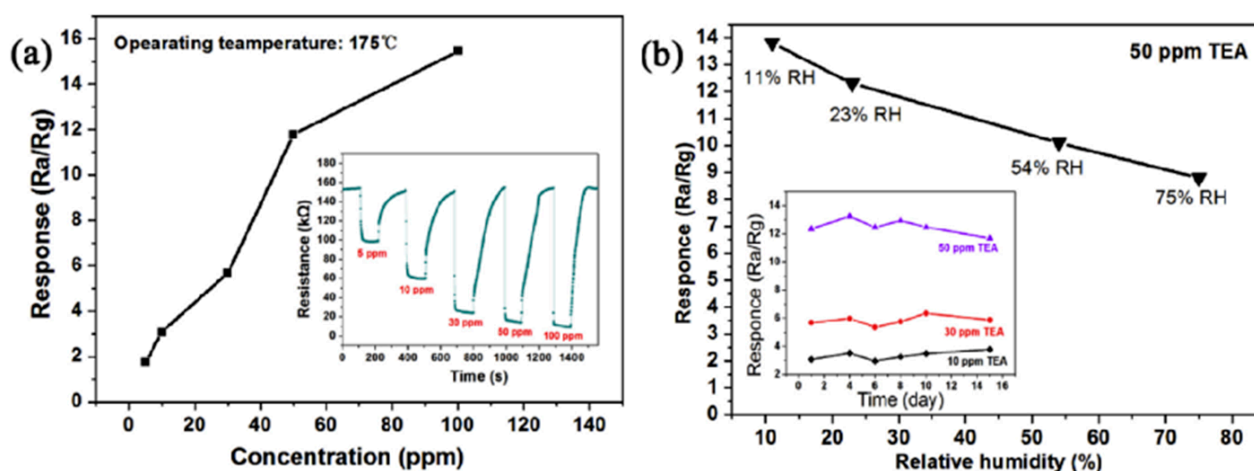


Figure 10. (a) A line chart of the relationship between the sensor response and the TEA concentration; (b) nanoparticle-based sensor responses to 50 ppm TEA under different RHs [88].

Zhang et al. [89] prepared Cr-doped SnO₂ microrods using a facile hydrothermal method to detect TEA. The gas sensitivity test found excellent selectivity and sensitivity to TEA; what was more surprising was its marvelous response time (1 s) as well as its humidity resistance. The latter above all makes it one good commercial sensor. In one recent study, Bi et al. [90] synthesized Rh-SnO₂ nanosheets by facile hydrothermal synthesis and subsequent surface impregnation precipitation and heat treatment. The sensor had better stability and gas selectivity, and its temperature response was nearly 15 times higher, than that of the nondoped sensor at the best working temperature (325 °C).

5.1.2. The Roles of Nonmetallic Elements

Adding nonmetallic elements to the material can reduce the Fermi level and enhance the electron transfer between the material and gas molecules, so as to improve the selectivity and sensitivity of the material to the target gas [91]. At present, some researchers have added carbon and other nonmetallic elements to gas-sensing materials to improve their gas-sensing properties [92].

To overcome the problems of high concentrations of chemical hydrothermal solutions and complex chemical reactions, Peng et al. [93] applied the magnetron sputtering process to prepare the core-shell structure and then combined it with reduced graphene oxide to prepare boron-doped reduced graphene oxide- (BRGO) coated Au@SnO₂. Figure 11 is the structure of the prepared materials. The enhancement of its gas-sensing properties

may be largely attributed to the wrapping with BRGO. In another report, Zhang et al. [94] prepared carbonized polymer dots doped with hierarchical tungsten to solve the problems of the high working temperature and high detection limit of TEA sensors. They not only developed the preparation method of the mixed material but also studied its gas-sensing performance to TEA and the effect of the carbon compound point on the performance improvement, which laid a foundation for the further study of carbon doping in the future.

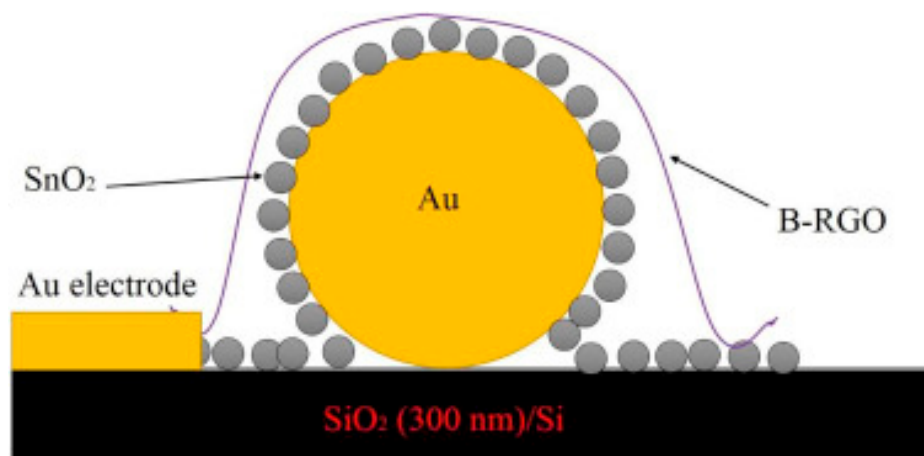


Figure 11. The schematic diagram of the B-RGO/SnO₂@Au heterostructure-based sensor [93].

5.2. Noble Metal Oxides and Transition Metal Oxides

Similar to the idea of using metals to enhance gas-sensing properties, the combination of different metal oxides can also improve gas-sensing performance [95]. In semiconductor physics, semiconductors with electrons as the main charge carriers are called n-type semiconductors, semiconductors with holes as the main charge carriers are called p-type semiconductors, and heterojunctions will be produced when different semiconductors contact [96]. Generally, the semiconductor oxides with different properties have different gas-sensing mechanisms and effects. According to investigations, common types of heterojunction are p-p, p-n, n-p, and hybrid junctions [97]. Because of the existence of heterojunctions, the material resistance is often very high, and in order to balance the Fermi level, it will produce a greater response when exposed to the target gas [98].

5.2.1. N-N Heterojunction

The n-type semiconductor metal compounds tend to have better gas-sensing performance and are the most used class of semiconductor metal compounds. Investigators have combined a large number of various n-type semiconductor compounds in an attempt to enhance their performance with TEA detection. The main principle of n-n heterojunction for enhancing the gas-sensing performance is as follows. The main carrier of n-n heterojunction is electrons, where the carriers will flow from the high side of the conduction band to the low side of the conduction band; an EDL is formed on the high side of the conduction band, and a charge accumulation layer is formed on the low side of the conduction band. This change will result in a larger response of the sensing material before and after exposure to the target gas with a larger range of electron changes [99].

Among the many examples, Xu et al. [100] prepared n-n heterojunctions via assembling SnO₂ nanosheets and TiO₂ nanoparticles employing the PLD method. They characterized the shape of the material by SEM and TEM, and they analyzed the elemental composition of the material by EDS, XRD, and XPS. The gas sensors were completely tested for several gas-sensing indexes such as repeatability, selectivity, and operating temperature. The test reports show that the sensor has not only excellent TEA selectivity but fast response time and recovery time. Xue et al. [101] prepared CeO₂/SnO₂ nanoflowers using the one-step hydrothermal method. The result shows that the response of 5 wt.% CeO₂ content

composite excellently improved. The sensing mechanism diagrams of pure SnO₂ and CeO₂/SnO₂ are shown in Figure 12.

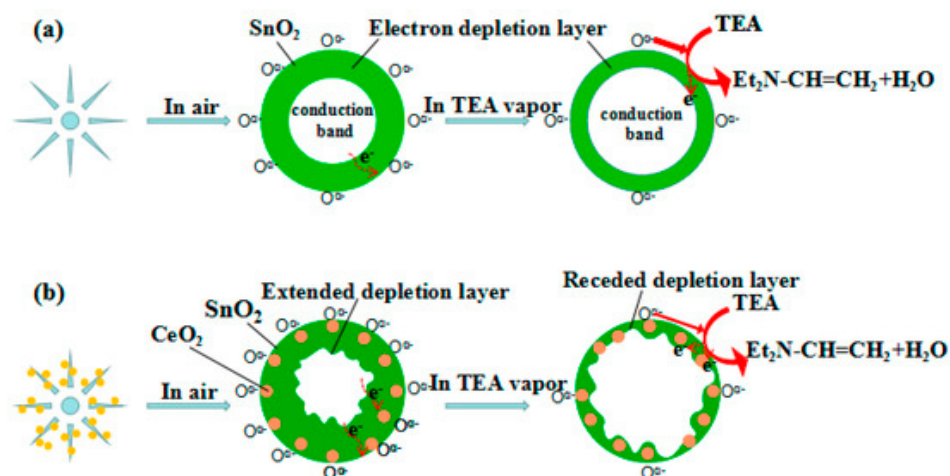


Figure 12. Sensing mechanism diagrams of (a) pure SnO₂ and (b) CeO₂/SnO₂ nanostructures [101].

5.2.2. P-P Heterojunction

Based on previous experimental experience, the gas-sensing performance of p-type semiconductor metal compounds is poor compared with that of n-type semiconductor metal compounds, but the gas sensing performance of p-type semiconductors can be relatively enhanced by forming p-p heterojunctions. The enhancement mechanism of the gas-sensing performance through p-p heterojunctions is mainly as follows. P-P heterojunctions have holes as the main carriers, in which the carriers will flow from the side with a higher valence band to the side with a lower valence band, forming a hole depletion layer on the side with a higher valence band and a hole accumulation layer on the side with a lower valence band [102]. The change in resistance due to this change is beneficial for the increase in gas-sensing performance [103].

Wang et al. [104] prepared NiWO₄@NiO p-p heterostructure via a self-sacrificing template method. The response of the heterojunction material prepared by the template was enhanced from 2.5 to 65 compared with pure NiO at an optimum operating temperature (240 °C) with 50 ppm of TEA gas. The team found that the p-p heterojunction needs to keep the balance of the Fermi energy level; electrons will be transferred from NiWO₄ to nickel monoxide, and the electron-hole pair recombination leads to higher resistance. The mechanism diagram is shown in Figure 13.

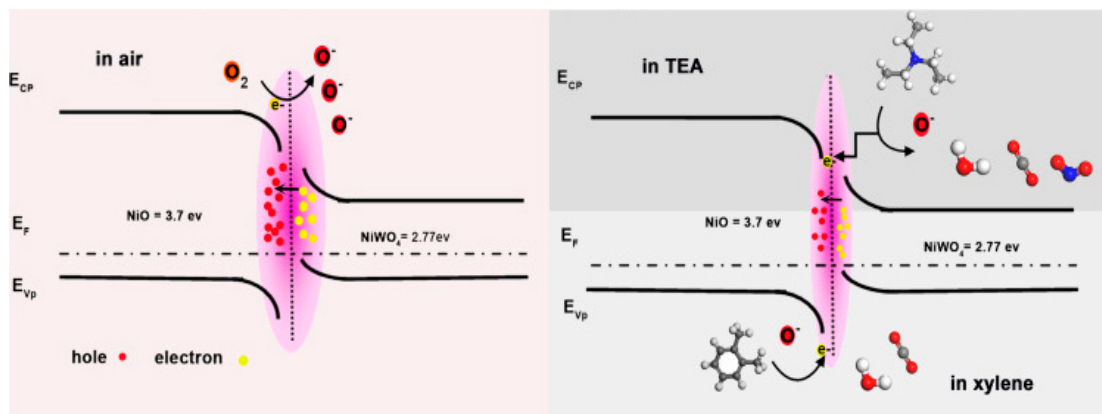


Figure 13. A schematic diagram of the improved gas-sensing mechanism of p-p NiWO₄ decorated NiO [104].

5.2.3. P-N Heterojunction

P-N heterojunctions, the most representative heterojunction, applied in a variety of different fields to enhance the physicochemical properties of semiconductors, are also one of the most important means of enhancing the TEA-sensing performance. P-N heterojunctions to improve gas-sensing performance are briefly described below. For p-n junction MOS sensing materials, the electron will migrate from n-type material to p-type material, and a large number of electrons are lost in the p-type material, forming a thick EDL, while holes are transferred to the p-type material, leading to band bending [105]. This process accelerates the carrier transfer efficiency in the accelerated material, so that the p-n heterojunction material obtains a higher resistance in the post-in and target gas reactor process to obtain the reaction-generated free electrons, lowering the resistance to obtain a large response [106].

For instance, Zeng et al. [107] fabricated a p-n heterojunction of $\text{Co}_3\text{O}_4/\text{WO}_3$ by a ZIF template. In this study, the sensor shows superb selectivity, excellent long-term stability, and a linear response for TEA. The authors explained the high performance of the sensor according to the large specific surface area, porosity, and most importantly, the depletion principle. In another study, Yu et al. [108] fabricated mesoporous and hierarchical hollow-structured In_2O_3 -NiO composites via solvothermal reaction and subsequent cation exchange. The result in Figure 14 shows the obvious descent of the working temperature. Figure 15 depicts the gas-sensing mechanisms as well as the energy band states of NiO, In_2O_3 , and In_2O_3 -NiO.

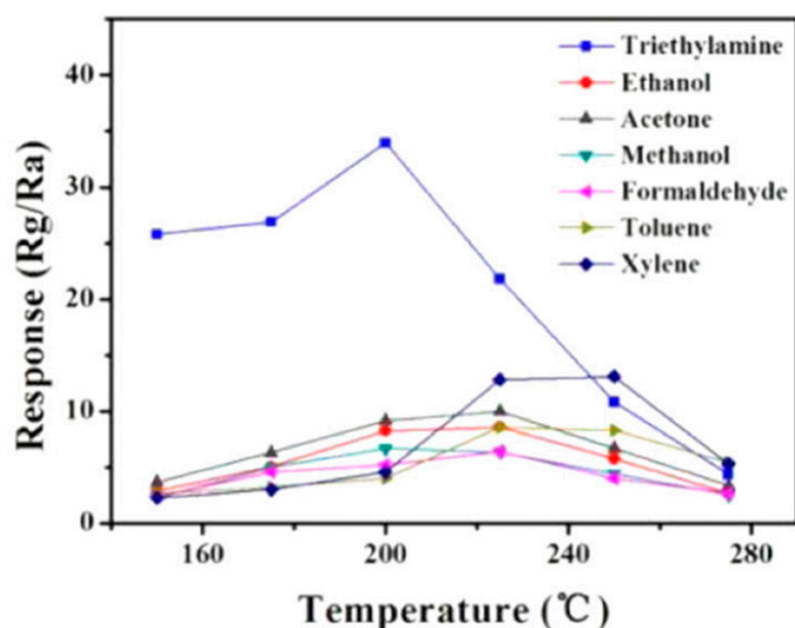


Figure 14. The selectivity of In_2O_3 -NiO composites to seven different VOCs at various temperatures [108].

5.3. Conducting Polymer

Although MOS materials are widely used as sensors, their high operating temperatures have always affected their practical applications. To solve the temperature problem, experimenters have begun to gradually apply conductive polymers in semiconductor gas sensors. Among them, the most widely used were the well-known polyaniline (PANI), polypyrrole (PPy), polythiophene (PT), and poly (3,4-ethylene dioxythiophene) (PEDOT). In 2016, Bai et al. [109] apply polyaniline to fabricate a TEA detection sensor. The fabricated polyaniline@ SnO_2 shows excellent selectivity and ultra-low detection temperature, which are the important performance indicators of TEA detection. This material opens the way to combining conducting polymer with semiconductor metal oxide for TEA detection.

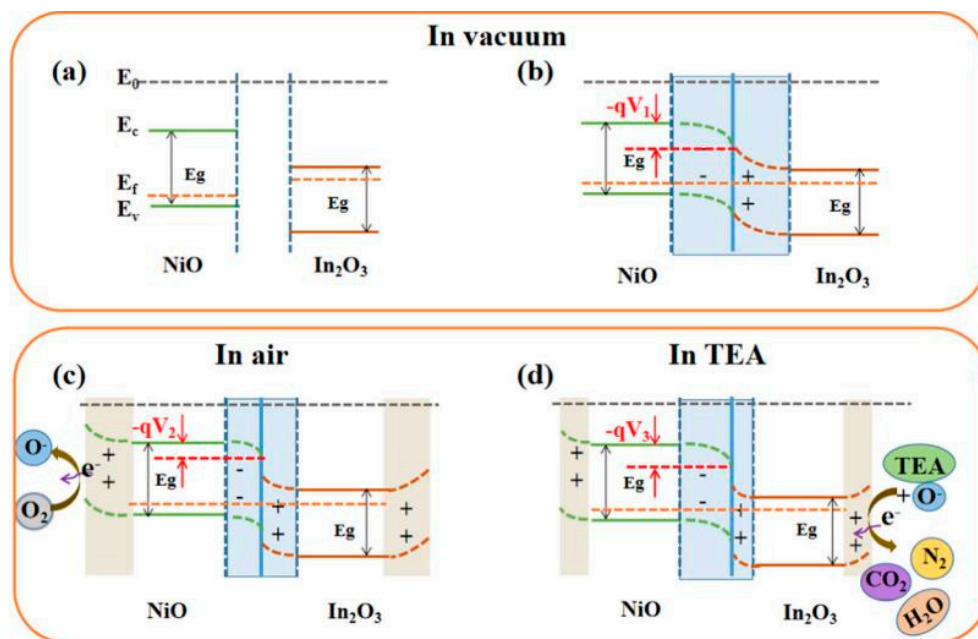


Figure 15. Schematic diagrams of the energy band states of NiO, In₂O₃, and In₂O₃-NiO, (a,b) in a vacuum, (c) in air, and (d) in TEA [108].

5.4. Quantum Dots

Quantum dots are one species of material used in chemiresistive sensors. Since their first introduction in 1983, scientists found that the bandgap properties of quantum dot materials can be changed by adjusting the quantum dot size. The materials have been applied in various fields including gradually in the sensing field [110]. In a report on TEA detection, Liu et al. [111] combined CdS quantum dots with ZnO to form a kind of n-n heterojunction structure, improving the response time (2 s) and decreasing the working temperature (200 °C). The following year, Liu et al. [112] again used quantum dots technology to combine CsPbBr₃ quantum dots with ZnO. This material has a higher response and lower detection limit compared with the previous experiment. The images of response versus temperature are exhibited in Figure 16. The two experiments by Liu et al. show that quantum dot materials have great potential for TEA detection, and more quantum dot materials may be used for TEA detection in the future.

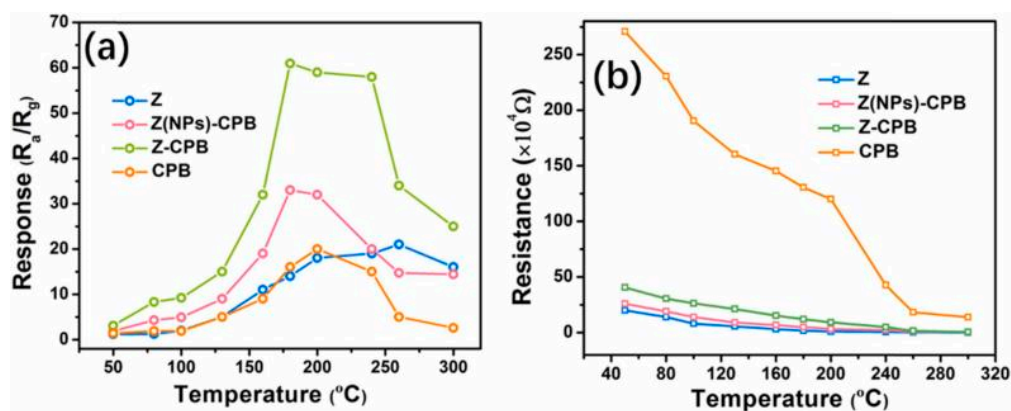


Figure 16. (a) Responses of as-obtained sensors versus different temperatures to 100 ppm of TEA. (b) The plots of Ra change for all sensors at different working temperatures to 100 ppm of TEA [112].

6. New Materials Application

Although conventional MOSs such as ZnO and SnO₂ have certain gas-sensing abilities, they are still difficult to work with at room temperature and have high detection limits, which hinders their practical application [113,114]. Therefore, it is imperative to find new materials to solve their existing problems. In recent years, graphene and its derivatives, carbon nanotubes, 2D transition metal carbides and nitrides (MXene), 2D transition metal dichalcogenide (TMDs), and spinel and perovskite materials have been gradually developed by scholars to enhance gas detection [115–117].

6.1. Graphene and Its Derivatives-Based

Graphene is a single-layer carbon sheet with a hexagonal filled lattice structure, which has many outstanding physical and chemical characteristics, such as good low temperature, high carrier mobility, excellent optical properties, large specific surface area, and excellent thermal conductivity [118]. The performance of graphene derivatives, graphene oxide (GO) and reduced graphene oxide (RGO) tablets, is further improved for their reactive oxygen groups [113,119]. Graphene and its derivatives combined with various functional materials are widely used in lithium-ion batteries, metal oxide supercapacitors, and other applications [120]. Because of its ability to adsorb gas at room temperature, large specific surface area, and high conductivity, graphene is also gradually being used in gas sensors [121].

Bai et al. [122] prepared a hybrid of pine dendritic BiVO₄/RGO via a one-step hydrothermal method enhancing the response of 10 ppm TEA at a working temperature of 180 °C. Figure 17 shows SEM images that indicate sufficient contact between the two materials and the full interaction of both. Figure 18 displays the nitrogen adsorption/desorption isotherm of BiVO₄/13.0 wt.% RGO hybrid; the figure reveals its large specific surface area, which is a benefit for TEA detection.

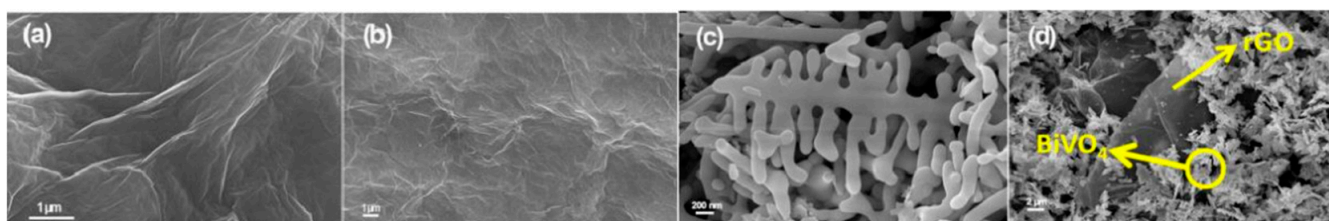


Figure 17. SEM images of (a) GO; (b) RGO; (c) pure pine dendritic BiVO₄; (d) BiVO₄/RGO hybrid [122].

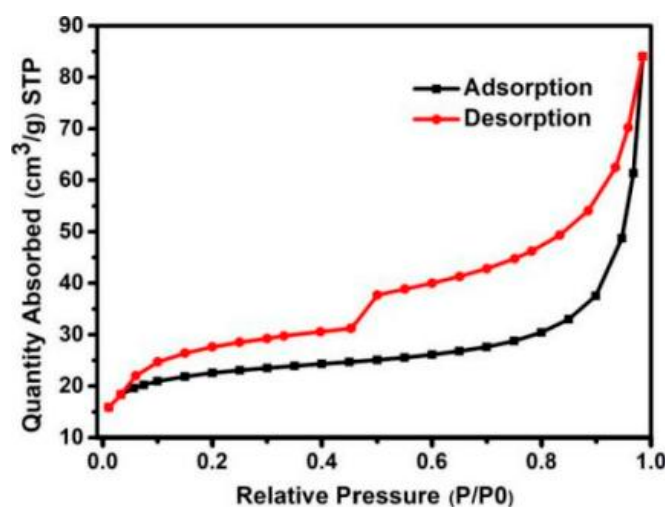


Figure 18. The nitrogen adsorption/desorption isotherm of BiVO₄/13.0 wt.% RGO hybrid [122].

Wei et al. [123] successfully prepared a MOF-derived α -Fe₂O₃ porous spindle combined with RGO using Fe-MIL-88 as a precursor through a simple solvothermal method to improve TEA sensing performance. Figure 19 presents dynamic response–recovery curves. It clearly shows that the new material decorated with RGO not only greatly increased response but accelerated response time. Responses of RGO/ α -Fe₂O₃ nanocomposites display better linearity and superior sensing performance.

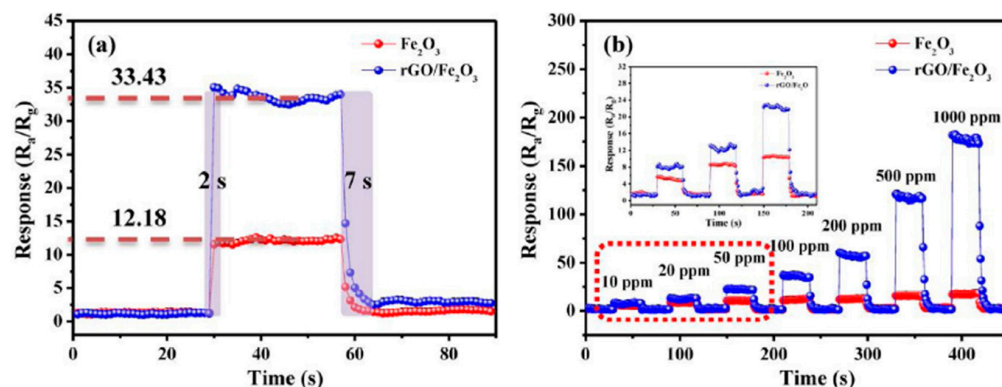


Figure 19. (a) Dynamic response–recovery curves (100 ppm TEA) of pure α -Fe₂O₃ spindles and RGO/ α -Fe₂O₃ nanocomposites at 280 °C. (b) Concentration-dependent response curves of pure α -Fe₂O₃ spindles and RGO/ α -Fe₂O₃ nanocomposites to 10–1000 ppm TEA [123].

Yu et al. [124] modified Co₃O₄ nanoparticles by wrapping RGO via a simple hydrothermal method. In their experiments, they found that Co₃O₄ with {100} crystal planes and {112} crystal planes could be prepared by changing the amount of sodium hydroxide. The experimental results show that the nanostructures with {112} surface contain more adsorbed oxygen, which can enhance the adsorption of TEA. Figure 20 shows the 3D electron density difference between the Co₃O₄ (100)/graphene interface and the Co₃O₄ (112)/graphene.

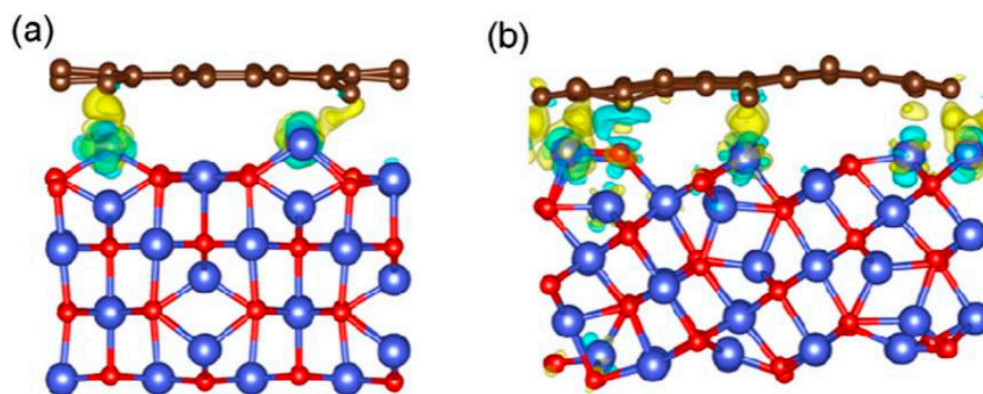


Figure 20. 3D electron density differences on the Co₃O₄ (100)/graphene interface (a) and the Co₃O₄ (112)/graphene interface (b). The cyan and yellow contours represent electron density depressions and accumulations, respectively [124].

6.2. MXenes-Based

Since the first MXene report in 2011, MXene materials have received extensive attention [125,126]. Various MXene materials such as Ti₃C₂T_x, Mo₂CT_x, and V₂CT_x have been successively prepared and gradually used in the research on gas sensors [127]. MXenes are early-transition metal carbides/carbonitrides and nitrides with a general formula M_{n+1}X_nT_x, where M represents transition metals (like Sc, Ti, V, Cr, Zr, Nb, Mo, and Ta), X is C or N, and T represents surface terminal groups (like O, F, and OH) [128].

MXene is a multifunctional material that is mostly used in catalysis, ion batteries, and gas storage [129]. Due to its special geometric and electronic structure, good conduc-

tivity, large specific surface area, excellent gas adsorption capacity, rich active sites, and excellent stability, it has been the focus of much attention in the field of gas sensing in recent years [130]. In one recent study, Liang et al. [131] applied MXene material for the first time to a TEA gas sensor and achieved a good response. They synthesized 2D/2D SnO₂ nanosheets/Ti₃C₂T_x MXene nanocomposites by a simple hydrothermal method and achieved fast response/recovery time, relatively high sensitivity, high stability, and excellent selectivity to the synergistic effect of SnO₂ and MXene in SNTM composite and its highly interconnected porous structure determine. Figure 21 is its XPS spectrum.

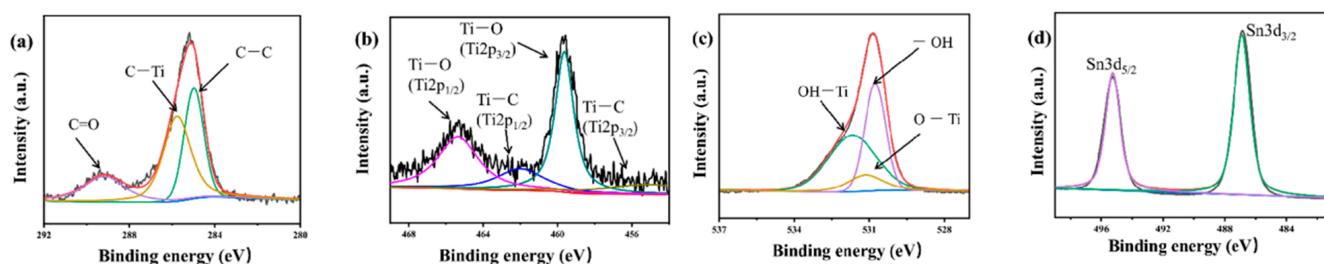


Figure 21. The high-resolution XPS spectra of (a) C 1s; (b) Ti 2p; (c) O 1s; (d) Sn 3d, respectively [131].

6.3. TMD-Based Materials

In addition to graphene and its derivatives as well as MXenes, 2D transition metal dichalcogenide (TMD) nanosheets are also applied in gas sensing. TMDs are a kind of layered material [132]. The basic chemical formula can be written as MX₂, where M represents transition metal elements, including Ti, V, Ta, Mo, and W, and X represents chalcogenide atoms (S, Se, Te, etc.); MoS₂, WS₂, MoSe₂, and WSe₂ are a few of the typical materials [133]. Because of its unique layered structure, large specific surface area, and excellent physicochemical as well as electronic properties, TMD has great application potential in the field of gas sensors [134].

However, there are few cases of its application in TEA detection. Xu et al. [135] proposed a novel n-n heterojunction material based on MoS₂/ZnO, and its size and microstructure were designed by controlling the annealing rate. They determined that the material remaining in a weak acid environment CTAB can gradually be adsorbed on MoS₂ nanosheets to form the n-n heterojunction. Then, they carefully researched its TEA sensing mechanism and enhanced the sensitivity by the unique microbridge structure. Yang et al. [136] studied the gas selectivity of 3D MoS₂/GO hybrid nanostructures under TEA and other VOCs. They found that the material had better selectivity for TEA gas at working temperature (260 °C). It may be that the synergistic effect of the layered TMDs and GO produce strange sensing characteristics. Figure 22 is the response curves.

6.4. Perovskite Structure and Spinel Structure

The general formula of perovskite structure is ABX₃, and the structure commonly used in gas sensors is ABO₃ [137,138]. Perovskite-type ternary compounds have a wide bandgap, excellent thermal stability, and chemical compositions including the partial substitution of A and/or B positions with aliovalent elements of variable sizes and values [139,140]. However, chemical instability, low porosity, and poor low-temperature stability hinder its application in gas sensors [141,142]. There are only a few perovskite materials applied to TEA sensing. Zheng et al. [143] obtained the CoSnO₃ nanoboxes via the calcination of CoSn(OH)₆ precursors derived from a solution-precipitation method. After a series of experiments, they came to the conclusion that the material is a kind of p-type semiconductor that can detect TEA under a low temperature with a low detection limit.

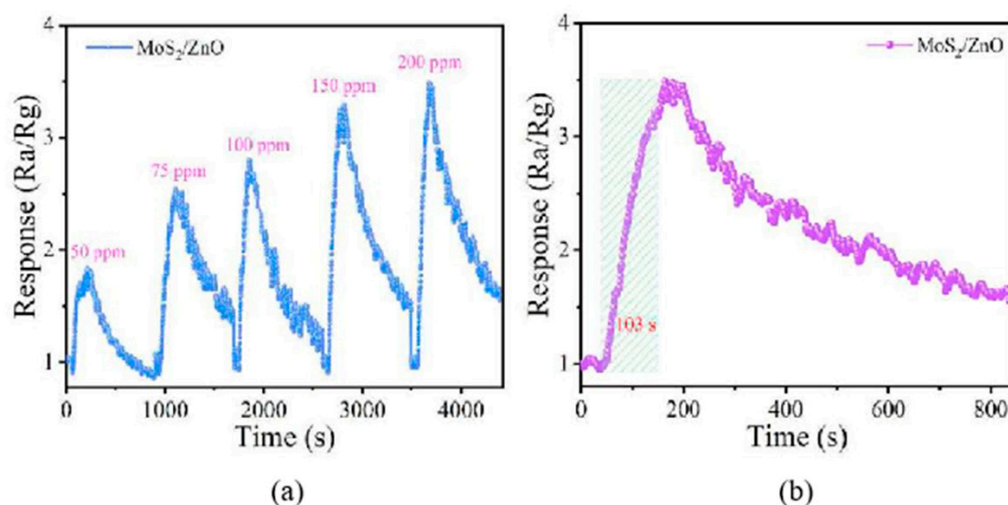


Figure 22. (a) The response curves of MoS₂/ZnO to different concentrations of TEA at room temperature. (b) The response–recovery curve of MoS₂/ZnO to 200 ppm TEA at room temperature [135].

Hao et al. [144] modified porous LaFeO₃ microspheres with RGO following a simple electrostatic self-assembly strategy. Figure 23a shows the sensing mechanism that the tight interface contact between LaFeO₃ microspheres and RGO tablets. RGO is wrapped on the surface of the microspheres to form p-p heterojunctions, causing the adsorbed oxygen to trap free electrons from the conductive band, in turn making the electrical resistance decrease. Figure 23b reveals the excellent selectivity of LaFeO₃, RGO/LaFeO₃ nanomaterials to 100 ppm of five different VOCs at 240 °C.

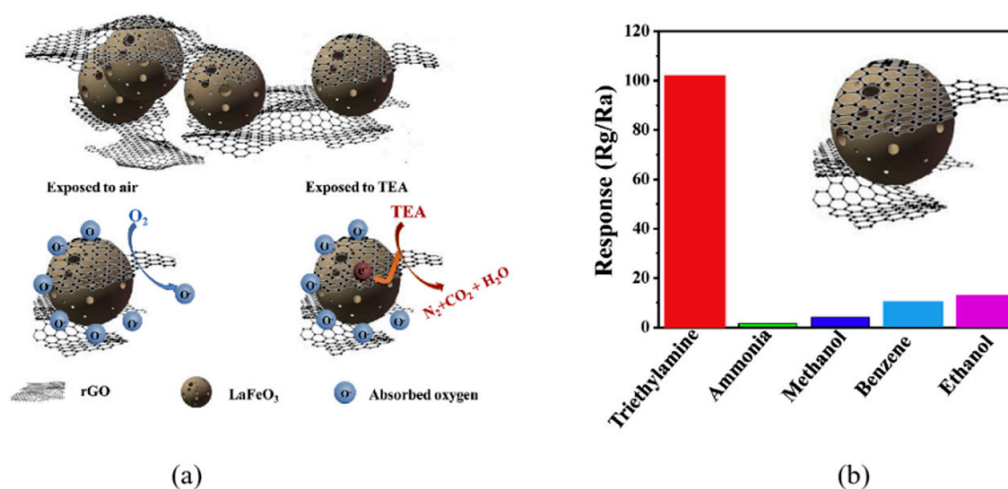


Figure 23. (a) The nanostructure and the possible gas-sensing mechanism of the RGO/LaFeO₃. (b) The response of LaFeO₃, RGO/LaFeO₃ to 100 ppm of five different VOCs at 240 °C [144].

In recent years, spinel structures have also been used in TEA gas detection because of their good thermal stability and sensitivity to VOCs [145,146]. The common formula for normal spinel structures is A^{tetra}(B₂)^{octa}O₄ where A is the distribution of positive second-order metal cations in tetrahedral voids, and B is the distribution of positive trivalent metal cations in octahedral voids [147]. The common formula for inverse spinel structures is B^{tetra}(AB)^{octa}O₄. The distribution of A and B is just the opposite of that normal spinel structure [148]. The different cation species and charge states of two sites in the polyhedral crystalline structure will significantly affect the physicochemical properties of nanomaterials [149]. Ma et al. [150] prepared hierarchical spinel-type corn-like MgAl₂O₄ (M = Ni, Co) architectures using a facile hydrothermal method and subsequent calcina-

tion. Subsequently, they completely and scientifically investigated the phase compositions and microstructures, which may be the essential influence factor of excellent gas-sensing properties. Yang et al. [151] investigated the impact of the calcination temperature on the morphology and TEA-sensing properties of NiCo_2O_4 microsphere nanomaterial. The experiment results reveal that the material shows good selectivity to TEA but that its high working temperature and slow response time need to be improved. The synthesis process and calcination results of NiCo_2O_4 micromaterials are displayed in Figure 24.

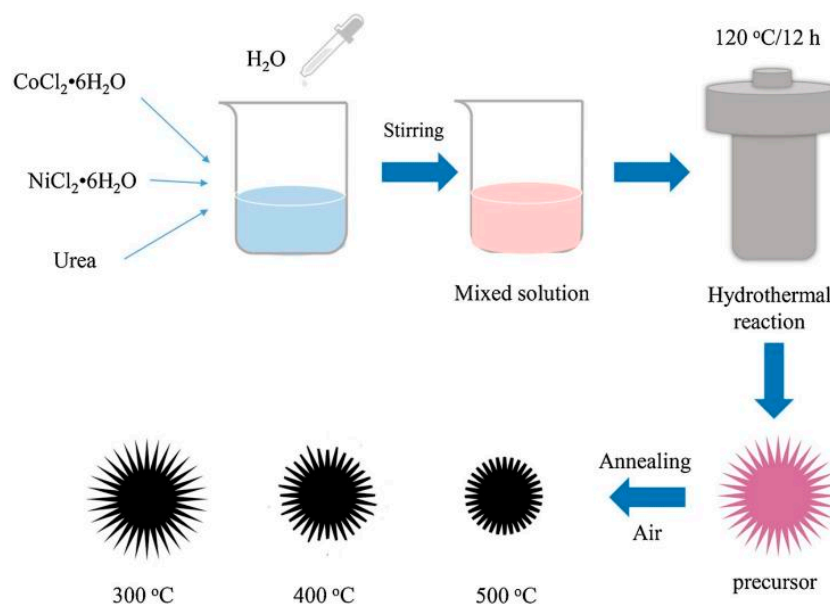


Figure 24. The synthesis process of NiCo_2O_4 nanospheres annealed at various temperatures [151].

The comparison of gas-sensing characteristics of nanomaterials listed in this paper will be given in Table 3 at the end of this section.

Table 3. The gas-sensing properties of various materials.

Nanomaterials	τ_{res}/τ_{rec} (s)	T (°C)	Conc. (ppm)	Res.	Lim. (ppm)	Ref.
Pine dendritic BiVO_4/RGO	5.9/11.4	180	10	5.9	2	[122]
$\alpha\text{-Fe}_2\text{O}_3$ porous spindle/RGO	2/7	280	50	24	-	[123]
$\text{Co}_3\text{O}_4/\text{RGO}$	-	25	100	10	-	[124]
2D/2D SnO_2 nanosheets/ $\text{Ti}_3\text{C}_2\text{T}_x$ MXene	1/1	140	50	33.4	5	[131]
MoS_2/ZnO bridge-like	35/142	200	100	31.08	0.097	[135]
MoS_2/GO hybrid nanostructures	7/11	260	1	2.8	1	[136]
CoSnO_3 nanoboxes	-	100	5	2.7	0.134	[143]
RGO-wrapped porous LaFeO_3 microspheres	3/4	240	50	103.5	1	[144]
corn-like MGA_2O_4 (M = Ni, Co)	136/41	270	100	7.6	-	[150]
Hierarchical NiCo_2O_4 microspheres	49/54	300	50	-	0.145	[151]

7. The Application of Advanced Instruments to Make Sensing Materials

The different fabrication methods of gas-sensing materials usually create different morphologies of the materials with different gas-sensing properties. Therefore, using some advanced equipment to prepare or modify sensing materials is also one typical way to improve gas-sensing properties. Generally, because of the simple synthesis operation, and low production costs, one-step hydrothermal [152] or solvothermal [153], sol-gel [154], and coprecipitation methods are popular. However, micromaterials prepared by atomic

layer deposition (ALD) [155], utilizing DC-sputtering technology, pulsed laser deposition (PLD) [156], or electrospinning [157] can achieve remarkable responses.

Take the ultrathin ZnO films (20 nm) as an example, Li et al. [158] prepared them by depositing ZnO on SiO₂ wafers by ALD. The preparation process for ALD deposition is exhibited in Figure 25a, and Figure 25b depicts the scheme of the Ar plasma process. The improvement of the TEA gas-sensing properties is attributed to oxygen vacancies acting as electron donors and multiple existing active sites. PLD is a technology that uses a laser to bombard a target material and deposit the bombarded plasma on the substrate for thin-film growth. The easy agreement with the target material composition is the biggest advantage of PLD, which is the main mark to distinguish it from other technologies. Moreover, the advantages of high deposition rate, short test cycle, high orientation, and high film resolution have allowed experimenters grow thin films using PLD for almost all materials [159]. Song et al. [160] successfully fabricated a kind of n-n heterojunction that combined ZnO nanorods with α -Fe₂O₃ nanoparticles by the PLD method. Superior response, lower detection concentration, and shorter response time of the material were caused by its larger specific surface area, which adsorbs more oxygen ions.

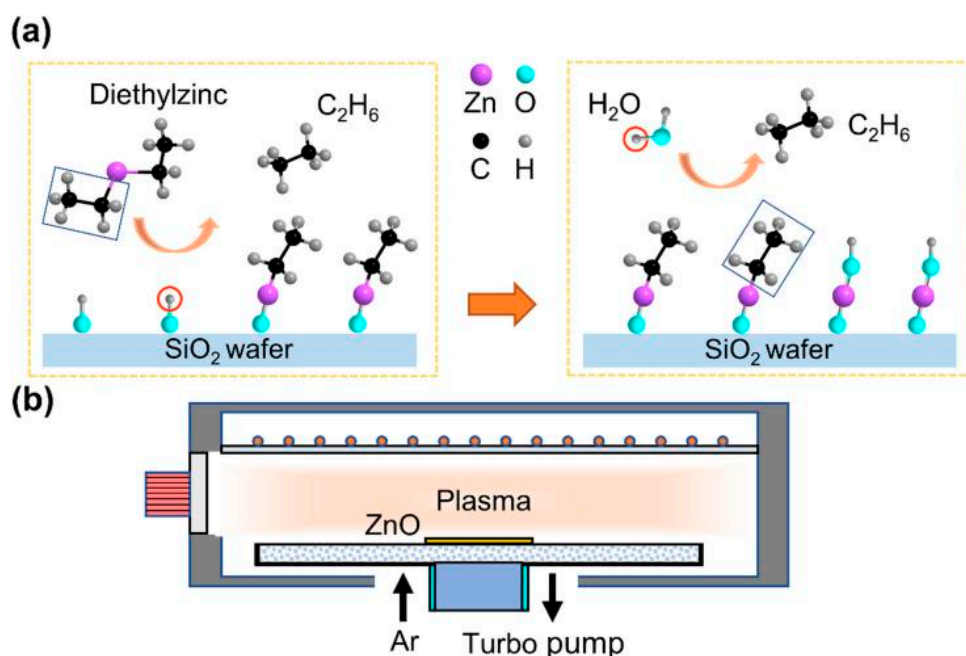


Figure 25. (a) ALD deposition process; (b) Ar plasma treatment [158].

Electrospinning is also a common method of preparing the nanofibers that are often used to obtain 1D nanoscale continuous fibers such as hollow fibers [161]. Because of the unique reaction process that mixes different materials into the electrospinning solution, the process can often yield 1D materials with good pore structure, large specific surface area, and excellent electron transport properties for a variety of applications [162]. A single needle electrospinning setup is drawn in Figure 26. Although electrospinning is efficient and convenient, there are few application examples in the manufacture of TEA gas sensors. One of the cases is Ma et al. [163], who fabricated several In₂O₃ hierarchical structure materials by electrospinning controlling calcination time and temperature. And the materials could be used in room temperature TEA detection, preserving superior sensitivity. A comprehensive analysis of the gas-sensing performance of the material was accomplished, and the team attributed the improved sensing performance to the unique material structure, multiple active sites, and special electron transmissions obtained by electrospinning.

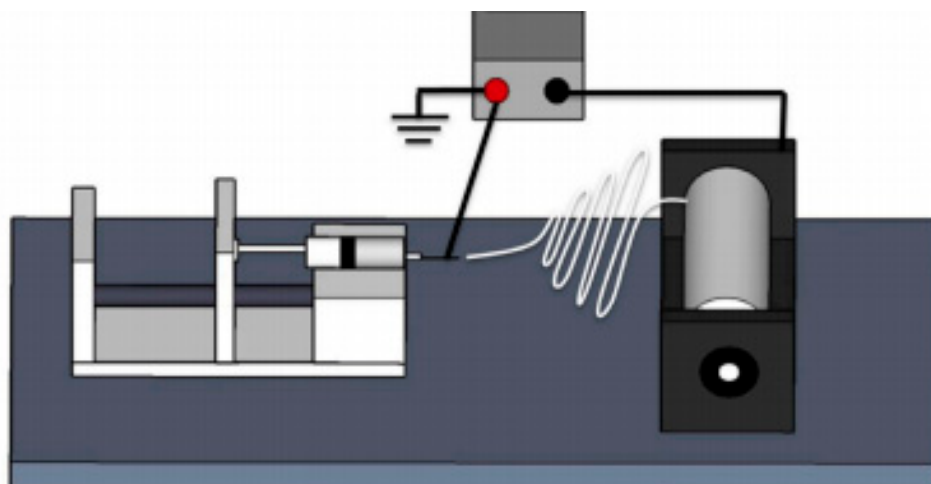


Figure 26. Schematic diagram of the electrospinning device [164].

A summary of the performance of the sensors manufactured with the various devices in this section is given in Table 4 at the end of this section.

Table 4. The gas-sensing properties of various materials fabricated by different devices.

Nanomaterials	τ_{res}/τ_{rec} (s)	T(°C)	Conc. (ppm)	Res.	Lim. (ppm)	Ref.
ultrathin ZnO films	531/46	180	10	1.8	-	[158]
α -Fe ₂ O ₃ nanoparticle/ZnO nanorod	4/86	300	50	63	1	[160]
InO ₂	184/-	40	50	87.8	5	[163]
SnO ₂	26/13	235	50	54.9	1	[165]

8. External Stimuli on Sensing Performance

In the practical application and production process of these sensors, we should not only consider the hard indexes such as the sensitivity, selectivity, and stability of the gas sensors to the target gas but factors such as the power consumption, repeatability, and manufacturing cost of the sensors. If the working temperature of a sensor can reach room temperature, the power consumption of the sensor will be greatly reduced, which can decrease both the fabricating and use costs. Decades ago, people began to look for auxiliary methods such as voltage biasing, UV light, and visible light excitons to enhance gas-sensing performance without relying on high temperature [166,167].

Liu et al. [168] investigated the enhancement of the TEA gas-sensing mechanism after the light irradiation of ZnO/ZnFe₂O₄ composites and developed a synthesis strategy by calcinating Zn₂Fe-LDH at different temperatures. The preparation process is shown in Figure 27a. The changing curves of sensor resistance after illumination are exhibited in Figure 27b. Clearly, light irradiation improves TEA gas sensing. Shanmugam et al. [169] reported an experiment with UV light to improve the gas adsorption properties of CeO₂ nanomaterials. The test result shows materials with higher TEA adsorption capacity compared with other VOCs attributable to Ov in the prepared CeO₂ NPs and photo-generated electron-hole pairs of the material. Yang et al. [170] investigated the impacts of ultraviolet light irradiation on ZnO-SnO₂ heterojunction nanobelts for TEA sensing. The conclusion is that under UV laser illumination, response/recovery times (1.8 s/18 s) significantly accelerate.

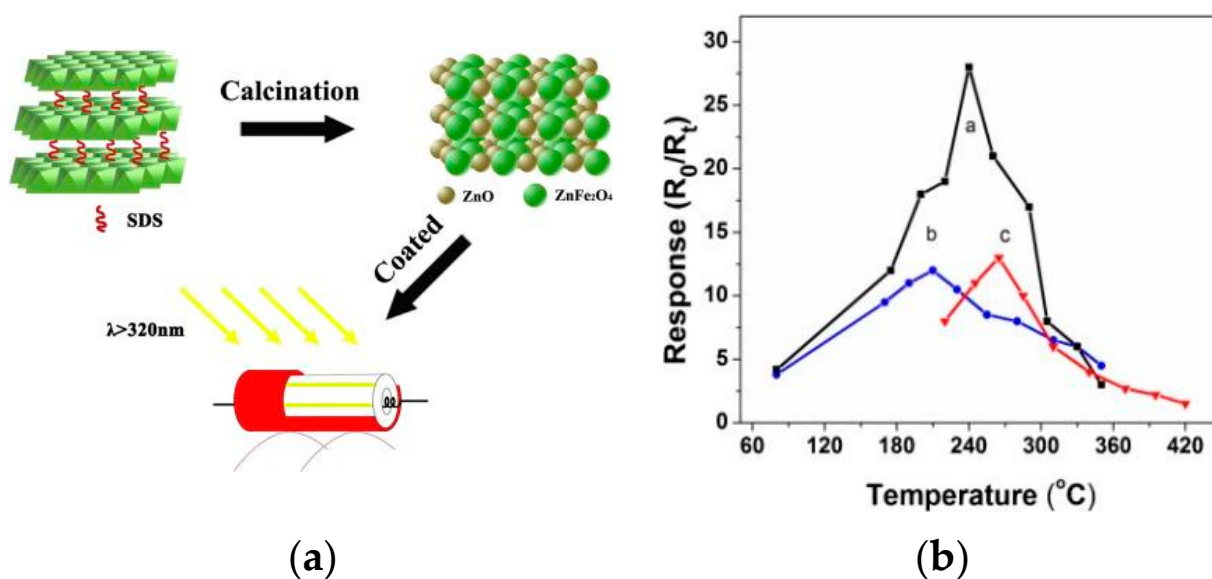


Figure 27. (a) The preparation and illumination of ZnO/ZnFe₂O₄. (b) The responses of ZnO/ZnFe₂O₄-600-a, ZnO/ZnFe₂O₄-800-b, and ZnO/ZnFe₂O₄-1000-c at various temperatures [168].

9. Conclusions and Outlook

Nanomaterial MOS sensors have gradually become an important development trend in gas detection. In this review paper, we briefly introduce the sensing characteristics of these gas sensors and two gas-sensing mechanisms for TEA detection. The major section of this review elaborates on several strategies to enhance the gas detection performance, such as the optimization of material structure, combining with other materials, using new materials, preparing materials with more advanced instruments, and stimulating the materials with external excitation.

In general, the alteration of the morphology and surface structure of materials can be either a dimensional increase to enlarge the specific surface area, porosity, and active adsorption sites for improved gas absorption or a change in the exposed crystal plane to improve gas selectivity and sensitivity. Various metal and nonmetal single elements can be doped into materials to improve gas-sensing performance due to their catalytic properties or electronic sensitization mechanisms. Other chemical compounds can also be incorporated to form p-p, p-n, and n-n heterojunctions to improve response. Recent advances also indicated the potential of quantum dot materials and conducting polymer materials in the optimization of sensitive performance. Furthermore, new materials such as graphene and its derivatives, MXenes (Ti₃C₂T_x, Mo₂CT_x, V₂CT_x), TMDs (MoS₂, WS₂, MoSe₂, and WSe₂), perovskite, and spinel materials are also used in TEA detection and possess unique characteristics such as reducing the working temperature. Advanced technology methods such as ALD and PLD also allow for preparing materials with better microstructures. Finally, external simulation can be an additional strategy for improving gas-sensing properties; for example, UV stimulation may allow gas-sensing materials to play an unexpected role.

Technology advances give rise to great numbers of materials with potential TEA-sensing capability, but further improvements are still in need. The previous summary illustrates that current TEA detection materials remain highly dependent on the traditional MOSs such as ZnO and SnO₂. However, there is still much room for improvement in its gas-sensing properties. First, the current poor response and selectivity of TEA gas materials should improve because many of the specific surface areas and porosities of these materials cannot adsorb enough target gas. Currently, polymetallic composites are becoming one of the main trends in TEA sensors, and the improvement of composite materials often increases the specific surface area and porosity of the material. Second,

the operating temperature of most TEA sensors is still high, most above 100 °C; graphene material is usually one of the choices to solve the high working temperature because of the unique properties of graphene composite materials. Third, many TEA-sensing materials are still in the laboratory stage, and practical TEA sensors that can be used in industrial production need to be developed and produced. This review provides a summary of existing techniques and materials and aims to improve the sensitivity performance of the TEA sensors, which may pave the way for the development of more advanced sensors in the future.

Author Contributions: Writing—review and editing, H.Z.; funding acquisition, F.M.; supervision, H.Z. and F.M.; investigation, Y.G.; resources, Y.G.; writing—original draft preparation, Y.G.; project administration, H.Z.; validation, H.Z. All authors have read and agreed to the published version of the manuscript.

Funding: This work was supported by the National Natural Science Foundation of China (62071112, 61833006 and 62033002) and the Fundamental Research Funds for the Central Universities in China (N2201008).

Institutional Review Board Statement: Not applicable.

Informed Consent Statement: Not applicable.

Data Availability Statement: Not applicable.

Conflicts of Interest: The authors declare no conflict of interest.

References

1. Yuan, Z.; Zhao, J.; Meng, F.; Qin, W.; Chen, Y.; Yang, M.; Ibrahim, M.; Zhao, Y. Sandwich-like composites of double-layer Co_3O_4 and reduced graphene oxide and their sensing properties to volatile organic compounds. *J. Alloys Compd.* **2019**, *793*, 24–30. [[CrossRef](#)]
2. Yun, P.; Ma, S.; Xu, X.; Wang, S.; Liu, W.; Wang, L.; Alhadi, A. Bi_2WO_6 nanoparticles-decorated ZnO nanosheets and their enhanced gas sensing properties. *Vacuum* **2021**, *194*, 110627. [[CrossRef](#)]
3. Yun, P.D.; Ma, S.Y.; Xu, X.L.; Wang, S.Y.; Han, T.; Sheng, H.; Pei, S.T.; Yang, T.T. Excellent triethylamine sensor with ultra-fast response and recovery time based on bulk Bi_2WO_6 material. *Mater. Lett.* **2021**, *285*, 129162. [[CrossRef](#)]
4. Li, C.B.; Xiao, F.; Xu, W.; Chu, Y.; Wang, Q.; Jiang, H.; Li, K.; Gao, X.W. Efficient self-photo-degradation of cationic textile dyes involved triethylamine and degradation pathway. *Chemosphere* **2021**, *266*, 129209. [[CrossRef](#)] [[PubMed](#)]
5. Wang, Z.; Lin, R.; Fang, W.; Li, G.; Guo, Y.; Qin, Z. Triethylamine as an initiator for cracking of heptane. *Energy* **2006**, *31*, 2773–2790. [[CrossRef](#)]
6. Yin, M.; Zhang, L.; Qiu, T.; Chen, Y.; Qi, S.; Wei, X.; Tian, X.; Ge, K.; Qiu, J.; Xu, D. Double-layer capsule of mesoporous ZnO@SnO_2 for sensitive detection of triethylamine. *Analyst* **2021**, *146*, 6193–6201. [[CrossRef](#)]
7. Brahmachari, G.; Nayek, N.; Nurjamil, K.; Karmakar, I.; Begam, S. Triethylamine—A Versatile Organocatalyst in Organic Transformations: A Decade Update. *Synthesis* **2018**, *50*, 4145–4164. [[CrossRef](#)]
8. Abbas, H.; Marappan, G.; Chidabaram, D.; Govindasamy, S.; Jayaraman Surya, V.; Sivalingam, Y. Graphene Oxide based Gas Sensor for Triethylamine Detection at Room Temperature. *IOP Conf. Ser. Mater. Sci. Eng.* **2022**, *1219*, 012031. [[CrossRef](#)]
9. Cai, T.; Chen, L.; Ren, Q.; Cai, S.; Zhang, J. The biodegradation pathway of triethylamine and its biodegradation by immobilized *Arthrobacter protophormiae* cells. *J. Hazard. Mater.* **2011**, *186*, 59–66. [[CrossRef](#)]
10. Xu, Y.; Ma, T.; Zheng, L.; Sun, L.; Liu, X.; Zhao, Y.; Zhang, J. Rational design of $\text{Au/Co}_3\text{O}_4$ -functionalized $\text{W}_{18}\text{O}_{49}$ hollow heterostructures with high sensitivity and ultralow limit for triethylamine detection. *Sens. Actuators B Chem.* **2019**, *284*, 202–212. [[CrossRef](#)]
11. Xu, Y.; Zheng, W.; Liu, X.; Zhang, L.; Zheng, L.; Yang, C.; Pinna, N.; Zhang, J. Platinum single atoms on tin oxide ultrathin films for extremely sensitive gas detection. *Mater. Horiz.* **2020**, *7*, 1519–1527. [[CrossRef](#)]
12. Ayad, M.M.; Torad, N.L. Quartz crystal microbalance sensor for detection of aliphatic amines vapours. *Sens. Actuators B Chem.* **2010**, *147*, 481–487. [[CrossRef](#)]
13. Filippio, E.; Manno, D.; Buccolieri, A.; Serra, A. Green synthesis of sucralose-capped silver nanoparticles for fast colorimetric triethylamine detection. *Sens. Actuators B Chem.* **2013**, *178*, 1–9. [[CrossRef](#)]
14. Moore, W.M.; Edwards, R.J.; Bavda, L.T. An Improved Capillary Gas Chromatography Method for Triethylamine. Application to Sarafloxacin Hydrochloride and GnRH Residual Solvents Testing. *Anal. Lett.* **1999**, *32*, 2603–2612. [[CrossRef](#)]
15. Majder-Łopaska, M.; Węsierski, T.; Dmochowska, A.; Salamowicz, Z.; Polańczyk, A. The Influence of Hydrogen on the Indications of the Electrochemical Carbon Monoxide Sensors. *Sustainability* **2019**, *12*, 14. [[CrossRef](#)]
16. Sun, Y.; Ding, W.; Li, J.; Jia, Y.; Guo, G.; Deng, Z. A novel and simple fluorescent chemical sensor SX based on AIE for relay recognition of Zn^{2+} and Cu^{2+} in aqueous system and analysis in logic gates. *J. Mol. Struct.* **2022**, *1252*, 132219. [[CrossRef](#)]

17. Promphet, N.; Ummartyotin, S.; Ngeontae, W.; Puthongkham, P.; Rodthongkum, N. Non-invasive wearable chemical sensors in real-life applications. *Anal. Chim. Acta* **2021**, *1179*, 338643. [[CrossRef](#)]
18. Gui, Y.; Zhao, J.; Wang, W.; Tian, J.; Zhao, M. Synthesis of hemispherical WO₃/graphene nanocomposite by a microwave-assisted hydrothermal method and the gas-sensing properties to triethylamine. *Mater. Lett.* **2015**, *155*, 4–7. [[CrossRef](#)]
19. Li, Q.; Li, Y.; Zeng, W. Preparation and Application of 2D MXene-Based Gas Sensors: A Review. *Chemosensors* **2021**, *9*, 225. [[CrossRef](#)]
20. Zhang, J.; Yu, Y.; Fang, P.; Liu, L.; Yue, H.; Ou, J.; Han, A. Anodization of aluminum in a sealed container. *Electrochem. Commun.* **2021**, *129*, 107086. [[CrossRef](#)]
21. Chu, X.; Chen, T.; Zhang, W.; Zheng, B.; Shui, H. Investigation on formaldehyde gas sensor with ZnO thick film prepared through microwave heating method. *Sens. Actuators B Chem.* **2009**, *142*, 49–54. [[CrossRef](#)]
22. Dey, A. Semiconductor metal oxide gas sensors: A review. *Mater. Sci. Eng. B* **2018**, *229*, 206–217. [[CrossRef](#)]
23. Xu, X.; Ma, S.; Xu, X.; Pei, S.; Han, T.; Liu, W. Transformation synthesis of heterostructured SnS₂/ZnS microspheres for ultrafast triethylamine detection. *J. Alloys Compd.* **2021**, *868*, 159286. [[CrossRef](#)]
24. Xu, K.; Zhan, C.; Zhao, W.; Yu, X.; Zhu, Q.; Yang, L. Tunable resistance of MOFs films via an anion exchange strategy for advanced gas sensing. *J. Hazard. Mater.* **2021**, *416*, 125906. [[CrossRef](#)] [[PubMed](#)]
25. Yang, T.; Yang, X.; Zhu, M.; Zhao, H.; Zhang, M. Coral-like ZnFe₂O₄-ZnO mesoporous heterojunction architectures: Synthesis and enhanced sensing properties for triethylamine. *Inorg. Chem. Front.* **2020**, *7*, 1918–1926. [[CrossRef](#)]
26. Zeb, S.; Cui, Y.; Zhao, H.; Sui, Y.; Yang, Z.; Khan, Z.U.; Ahmad, S.M.; Ikram, M.; Gao, Y.; Jiang, X. Synergistic Effect of Au-PdO Modified Cu-Doped K₂W₄O₁₃ Nanowires for Dual Selectivity High Performance Gas Sensing. *ACS Appl. Mater. Interfaces* **2022**, *14*, 13836–13847. [[CrossRef](#)] [[PubMed](#)]
27. Gong, F.-L.; Peng, M.-X.; Yue, L.-J.; Chen, J.-L.; Xie, K.-F.; Zhang, Y.-H. Design of p-n heterojunction on mesoporous ZnO/Co₃O₄ nanosheets for triethylamine sensor. *Chem. Phys. Lett.* **2021**, *779*, 138891. [[CrossRef](#)]
28. Shao, S.; Xie, C.; Xia, Y.; Zhang, L.; Zhang, J.; Wei, S.; Kim, H.W.; Kim, S.S. Highly conjugated three-dimensional van der Waals heterostructure-based nanocomposite films for ultrahigh-responsive TEA gas sensors at room temperature. *J. Mater. Chem. A* **2022**, *10*, 2995–3008. [[CrossRef](#)]
29. Zhang, Y.-H.; Wang, C.-N.; Gong, F.-L.; Chen, J.-L.; Xie, K.-F.; Zhang, H.-L.; Fang, S.-M. Ultra-sensitive triethylamine sensors based on oxygen vacancy-enriched ZnO/SnO₂ micro-camellia. *J. Mater. Chem. C* **2021**, *9*, 6078–6086. [[CrossRef](#)]
30. Liu, L.; Zhao, Y.; Song, P.; Yang, Z.; Wang, Q. ppb level triethylamine detection of yolk-shell SnO₂/Au/Fe₂O₃ nanoboxes at low-temperature. *Appl. Surf. Sci.* **2019**, *476*, 391–401. [[CrossRef](#)]
31. Li, Z.; Xiong, Y.; Bi, D.; Liu, Q.; Yang, C.; Zhang, J. Continuously improved gas-sensing performance of Zn₂SnO₄ porous octahedrons by structure evolution and further ZnSnO₃ nanosheets decoration. *J. Alloys Compd.* **2022**, *901*, 163744. [[CrossRef](#)]
32. Xiong, Y.; Liu, W.; Qiao, X.; Song, X.; Wang, S.; Zhang, X.; Wang, X.; Tian, J. Confined synthesis of 2D ultrathin ZnO/Co₃O₄ nanomeshes heterostructure for superior triethylamine detection at low temperature. *Sens. Actuators B Chem.* **2021**, *346*, 130486. [[CrossRef](#)]
33. Liang, X.; Zhang, J.; Zhang, K.; Yang, X.; Zhang, M. The modification effect of Fe₂O₃ nanoparticles on ZnO nanorods improves the adsorption and detection capabilities of TEA. *Inorg. Chem. Front.* **2022**, *9*, 259–266. [[CrossRef](#)]
34. Jin, Q.; Wen, W.; Wang, Z.-X.; Wang, R.-H.; Zheng, S.; Ye, Z.; Wu, J.-M. Nanoarchitectonics of nest-like MnO₂/TiO₂ thin film for triethylamine sensing. *Sens. Actuators B Chem.* **2022**, *353*, 131137. [[CrossRef](#)]
35. Meng, L.; Bu, W.; Li, Y.; Qin, Q.; Zhou, Z.; Hu, C.; Chuai, X.; Wang, C.; Sun, P.; Lu, G. Highly selective triethylamine sensing based on SnO/SnO₂ nanocomposite synthesized by one-step solvothermal process and sintering. *Sens. Actuators B Chem.* **2021**, *342*, 130018. [[CrossRef](#)]
36. Meng, F.; Liao, Z.; Xing, C.; Yuan, Z.; Zhang, R.; Zhu, H.; Li, J. Preparation of SnO₂/SiO₂ nanocomposites by sol-gel method for enhancing the gas sensing performance to triethylamine. *J. Alloys Compd.* **2022**, *893*, 162189. [[CrossRef](#)]
37. Liu, J.; Zhang, L.; Fan, J.; Yu, J. Semiconductor Gas Sensor for Triethylamine Detection. *Small* **2022**, *18*, e2104984. [[CrossRef](#)]
38. Yang, J.; Han, W.; Ma, J.; Wang, C.; Shimanoe, K.; Zhang, S.; Sun, Y.; Cheng, P.; Wang, Y.; Zhang, H.; et al. Sn doping effect on NiO hollow nanofibers based gas sensors about the humidity dependence for triethylamine detection. *Sens. Actuators B Chem.* **2021**, *340*, 129971. [[CrossRef](#)]
39. Fan, Y.; Xu, Y.; Wang, Y.; Sun, Y. Fabrication and characterization of Co-doped ZnO nanodiscs for selective TEA sensor applications with high response, high selectivity and ppb-level detection limit. *J. Alloys Compd.* **2021**, *876*, 160170. [[CrossRef](#)]
40. Yang, J.; Li, X.; Wu, J.; Han, Y.; Wang, Z.; Zhang, X.; Xu, Y. Yolk-shell (Cu,Zn)Fe₂O₄ ferrite nano-microspheres with highly selective triethylamine gas-sensing properties. *Dalton Trans.* **2020**, *49*, 14475–14482. [[CrossRef](#)]
41. Ma, N.N.; Ma, S.Y.; Wang, L.; Wang, X.P.; Liu, M.M.; Cai, Y.H.; Yang, T.T. Design a SnWO₄ coral-like nanostructure for triethylamine (TEA) sensing. *Vacuum* **2022**, *198*, 110913. [[CrossRef](#)]
42. Ji, H.; Zeng, W.; Li, Y. Gas sensing mechanisms of metal oxide semiconductors: A focus review. *Nanoscale* **2019**, *11*, 22664–22684. [[CrossRef](#)] [[PubMed](#)]
43. Kong, D.; Han, J.; Gao, Y.; Gao, Y.; Zhou, W.; Liu, G.; Lu, G. Lower coordination Co₃O₄ mesoporous hierarchical microspheres for comprehensive sensitization of triethylamine vapor sensor. *J. Hazard. Mater.* **2022**, *430*, 128469. [[CrossRef](#)]

44. Song, X.; Xu, Q.; Zhang, T.; Song, B.; Li, C.; Cao, B. Room-temperature, high selectivity and low-ppm-level triethylamine sensor assembled with Au decahedrons-decorated porous α -Fe₂O₃ nanorods directly grown on flat substrate. *Sens. Actuators B Chem.* **2018**, *268*, 170–181. [[CrossRef](#)]
45. Liu, H.; Cao, X.; Wu, H.; Li, B.; Li, Y.; Zhu, W.; Yang, Z.; Huang, Y. Innovative development on a p-type delafossite CuCrO₂ nanoparticles based triethylamine sensor. *Sens. Actuators B Chem.* **2020**, *324*, 128743. [[CrossRef](#)]
46. Wang, T.; Wang, X.; Wang, Y.; Yi, G.; Shi, C.; Yang, Y.; Sun, G.; Zhang, Z. Construction of Zn₂SnO₄ decorated ZnO nanoparticles for sensing triethylamine with dramatically enhanced performance. *Mater. Sci. Semicond. Process.* **2022**, *140*, 106403. [[CrossRef](#)]
47. Hu, Q.; He, J.; Chang, J.; Gao, J.; Huang, J.; Feng, L. Needle-Shaped WO₃ Nanorods for Triethylamine Gas Sensing. *ACS Appl. Nano Mater.* **2020**, *3*, 9046–9054. [[CrossRef](#)]
48. Chu, X.; Liang, S.; Sun, W.; Zhang, W.; Chen, T.; Zhang, Q. Trimethylamine sensing properties of sensors based on MoO₃ microrods. *Sens. Actuators B Chem.* **2010**, *148*, 399–403. [[CrossRef](#)]
49. Liu, F.; Chen, X.; Wang, X.; Han, Y.; Song, X.; Tian, J.; He, X.; Cui, H. Fabrication of 1D Zn₂SnO₄ nanowire and 2D ZnO nanosheet hybrid hierarchical structures for use in triethylamine gas sensors. *Sens. Actuators B Chem.* **2019**, *291*, 155–163. [[CrossRef](#)]
50. Zhai, T.; Xu, H.; Li, W.; Yu, H.; Chen, Z.; Wang, J.; Cao, B. Low-temperature in-situ growth of SnO₂ nanosheets and its high triethylamine sensing response by constructing Au-loaded ZnO/SnO₂ heterostructure. *J. Alloys Compd.* **2018**, *737*, 603–612. [[CrossRef](#)]
51. Jin, X.; Li, Y.; Zhang, B.; Xu, X.; Sun, G.; Wang, Y. Temperature-dependent dual selectivity of hierarchical porous In₂O₃ nanospheres for sensing ethanol and TEA. *Sens. Actuators B Chem.* **2021**, *330*, 129271. [[CrossRef](#)]
52. Ma, Q.; Chu, S.; Li, H.; Guo, J.; Zhang, Q.; Lin, Z. Flower-like In₂O₃/ZnO heterostructure with accelerated multi-orientation electron transport mechanism for superior triethylamine detection. *Appl. Surf. Sci.* **2021**, *569*, 151074. [[CrossRef](#)]
53. Cai, Y.H.; Ma, S.Y.; Yang, T.T.; Cao, P.F.; Wang, L.; Sheng, H.; Liu, M.M. Preparation of YVO₄ octahedral nanomaterials and gas-sensing characteristics to triethylamine. *J. Alloys Compd.* **2022**, *897*, 163167. [[CrossRef](#)]
54. Sá, B.S.; Zito, C.A.; Perfecto, T.M.; Volanti, D.P. Porous ZnSnO₃ nanocubes as a triethylamine sensor. *Sens. Actuators B Chem.* **2021**, *338*, 129869. [[CrossRef](#)]
55. Ji, H.; Qin, W.; Yuan, Z.; Meng, F. Qualitative and quantitative recognition method of drug-producing chemicals based on SnO₂ gas sensor with dynamic measurement and PCA weak separation. *Sens. Actuators B Chem.* **2021**, *348*, 130698. [[CrossRef](#)]
56. Ma, Q.; Chu, S.; Li, H.; Guo, J.; Zhang, Q. Cubic-like In₂O₃/α-Fe₂O₃ heterostructures assembled with 2D porous nanoplates for superior triethylamine gas-sensing behavior. *Mater. Lett.* **2021**, *302*, 130452. [[CrossRef](#)]
57. Yu, Q.; Kong, W.; Zhang, Y.; Li, X.; Xu, Y. Morphology-controllable synthesis of hierarchical hollow GaFeO₃ microcubes with selective triethylamine gas-sensing properties. *Ceram. Int.* **2022**, *48*, 4554–4562. [[CrossRef](#)]
58. Meng, X.; Yao, M.; Mu, S.; Wang, Y. Oxygen Vacancies Enhance Triethylamine Sensing Properties of SnO₂ Nanoparticles. *ChemistrySelect* **2019**, *4*, 11268–11274. [[CrossRef](#)]
59. Du, J.; Zhao, R.; Xie, Y.; Li, J. Size-controlled synthesis of SnO₂ quantum dots and their gas-sensing performance. *Appl. Surf. Sci.* **2015**, *346*, 256–262. [[CrossRef](#)]
60. Li, T.; Zeng, W.; Wang, Z. Quasi-one-dimensional metal-oxide-based heterostructural gas-sensing materials: A review. *Sens. Actuators B Chem.* **2015**, *221*, 1570–1585. [[CrossRef](#)]
61. Zhao, S.; Shen, Y.; Yan, X.; Zhou, P.; Yin, Y.; Lu, R.; Han, C.; Cui, B.; Wei, D. Complex-surfactant-assisted hydrothermal synthesis of one-dimensional ZnO nanorods for high-performance ethanol gas sensor. *Sens. Actuators B Chem.* **2019**, *286*, 501–511. [[CrossRef](#)]
62. Meng, F.; Shi, X.; Yuan, Z.; Ji, H.; Qin, W.; Shen, Y.; Xing, C. Detection of four alcohol homologue gases by ZnO gas sensor in dynamic interval temperature modulation mode. *Sens. Actuators B Chem.* **2022**, *350*, 130867. [[CrossRef](#)]
63. Yang, X.; Zhang, S.; Yu, Q.; Zhao, L.; Sun, P.; Wang, T.; Liu, F.; Yan, X.; Gao, Y.; Liang, X.; et al. One step synthesis of branched SnO₂/ZnO heterostructures and their enhanced gas-sensing properties. *Sens. Actuators B Chem.* **2019**, *281*, 415–423. [[CrossRef](#)]
64. Lv, Y.-z.; Li, C.-r.; Guo, L.; Wang, F.-c.; Xu, Y.; Chu, X.-f. Triethylamine gas sensor based on ZnO nanorods prepared by a simple solution route. *Sens. Actuators B Chem.* **2009**, *141*, 85–88. [[CrossRef](#)]
65. Liu, B.; Yang, H.; Zhao, H.; An, L.; Zhang, L.; Shi, R.; Wang, L.; Bao, L.; Chen, Y. Synthesis and enhanced gas-sensing properties of ultralong NiO nanowires assembled with NiO nanocrystals. *Sens. Actuators B Chem.* **2011**, *156*, 251–262. [[CrossRef](#)]
66. Zou, Y.; Chen, S.; Sun, J.; Liu, J.; Che, Y.; Liu, X.; Zhang, J.; Yang, D. Highly Efficient Gas Sensor Using a Hollow SnO₂ Microfiber for Triethylamine Detection. *ACS Sens.* **2017**, *2*, 897–902. [[CrossRef](#)]
67. Lei, G.; Li, Z.; Lu, G.; Hu, J.; Shang, H.; Zhang, X.; Liu, X.; Zhang, J.; Guo, X. Tungsten oxide thin films for highly sensitive triethylamine detection. *J. Mater.* **2022**, *8*, 408–416. [[CrossRef](#)]
68. Zhang, L.; Yin, M.; Qiu, J.; Qiu, T.; Chen, Y.; Qi, S.; Wei, X.; Tian, X.; Xu, D. Mesoporous ZnO nanosheet as gas sensor for sensitive triethylamine detection. *Anal Bioanal. Chem.* **2022**, *414*, 2181–2188. [[CrossRef](#)]
69. Liu, Y.; Liu, H.; Hu, A.; Wei, Y.; Ou, W.; Deng, X.; Wang, S.; Yu, K. An efficient low-temperature triethylamine gas sensor based on 2D ultrathin SnO₂ nanofilms. *Semicond. Sci. Technol.* **2021**, *36*, 125022. [[CrossRef](#)]
70. Zhang, J.; Zhang, B.; Yao, S.; Li, H.; Chen, C.; Bala, H.; Zhang, Z. Improved triethylamine sensing properties of fish-scale-like porous SnO₂ nanosheets by decorating with Ag nanoparticles. *J. Mater.* **2022**, *8*, 518–525. [[CrossRef](#)]
71. Zhao, S.; Shen, Y.; Zhou, P.; Zhong, X.; Han, C.; Zhao, Q.; Wei, D. Design of Au@WO₃ core-shell structured nanospheres for ppb-level NO₂ sensing. *Sens. Actuators B Chem.* **2019**, *282*, 917–926. [[CrossRef](#)]

72. Meng, F.; Qi, T.; Zhang, J.; Zhu, H.; Yuan, Z.; Liu, C.; Qin, W.; Ding, M. MoS₂-Templated Porous Hollow MoO₃ Microspheres for Highly Selective Ammonia Sensing via a Lewis Acid-Base Interaction. *IEEE Trans. Ind. Electron.* **2022**, *69*, 960–970. [CrossRef]
73. Wang, J.; Pei, C.; Cheng, L.; Wan, W.; Zhao, Q.; Yang, H.; Liu, S. Responses of three-dimensional porous ZnO foam structures to the trace level of triethylamine and ethanol. *Sens. Actuators B Chem.* **2016**, *223*, 650–657. [CrossRef]
74. Zhai, C.; Zhu, M.; Jiang, L.; Yang, T.; Zhao, Q.; Luo, Y.; Zhang, M. Fast triethylamine gas sensing response properties of nanosheets assembled WO₃ hollow microspheres. *Appl. Surf. Sci.* **2019**, *463*, 1078–1084. [CrossRef]
75. Sui, L.-I.; Xu, Y.-M.; Zhang, X.-F.; Cheng, X.-L.; Gao, S.; Zhao, H.; Cai, Z.; Huo, L.-H. Construction of three-dimensional flower-like α -MoO₃ with hierarchical structure for highly selective triethylamine sensor. *Sens. Actuators B Chem.* **2015**, *208*, 406–414. [CrossRef]
76. Yuan, Y.; Wang, Y.; He, X.; Chen, M.; Liu, J.; Liu, B.; Zhao, H.; Liu, S.; Yang, H. Increasing gas sensitivity of Co₃O₄ octahedra by tuning Co-Co₃O₄ surface structure and sensing mechanism of 3-coordinated Co atom as an active center. *J. Mater. Sci. Mater. Electron.* **2020**, *31*, 8852–8864. [CrossRef]
77. Xiang, R.; Zhang, L.; Guo, J.; Wang, Y.; Yuan, Y.; Wang, Y.; Chen, M.; Qi, C.; Liu, B.; Zhao, H.; et al. Enhanced gas sensing performances of hydrogenated MnO octahedrons with {111} facets and the sensing mechanism of unsaturated Mn as a reactive atom. *J. Alloys Compd.* **2021**, *884*, 160872. [CrossRef]
78. Xu, H.-Y.; Chen, Z.-R.; Liu, C.-Y.; Ye, Q.; Yang, X.-P.; Wang, J.-Q.; Cao, B.-Q. Preparation of {200} crystal faced SnO₂ nanorods with extremely high gas sensitivity at lower temperature. *Rare Met.* **2021**, *40*, 2004–2016. [CrossRef]
79. Wang, J.; Zhang, Z.; Rettig, O. Triethylamine sensing characteristics of nonpolar (11–20) and polar (0001) GaN thin films. *Sens. Actuators B Chem.* **2021**, *329*, 129237. [CrossRef]
80. Bai, S.; Zuo, Y.; Zhang, K.; Zhao, Y.; Luo, R.; Li, D.; Chen, A. WO₃-ZnFe₂O₄ heterojunction and rGO decoration synergistically improve the sensing performance of triethylamine. *Sens. Actuators B Chem.* **2021**, *347*, 130619. [CrossRef]
81. Guo, L.; Wang, Y.; Shang, Y.; Yang, X.; Zhang, S.; Wang, G.; Wang, Y.; Zhang, B.; Zhang, Z. Preparation of Pd/PdO@ZnO-ZnO nanorods by using metal organic framework templated catalysts for selective detection of triethylamine. *Sens. Actuators B Chem.* **2022**, *350*, 130840. [CrossRef]
82. Li, G.; Ma, Z.; Hu, Q.; Zhang, D.; Fan, Y.; Wang, X.; Chu, X.; Xu, J. PdPt Nanoparticle-Functionalized α -Fe₂O₃ Hollow Nanorods for Triethylamine Sensing. *ACS Appl. Nano Mater.* **2021**, *4*, 10921–10930. [CrossRef]
83. Zeng, J.; Rong, Q.; Xiao, B.; Yu, R.; Zi, B.; Kuang, X.; Deng, X.; Ma, Y.; Zhang, J.; Wu, J.; et al. Single-atom silver loaded on tungsten oxide with oxygen vacancies for high performance triethylamine gas sensors. *J. Mater. Chem. A* **2021**, *9*, 8704–8710. [CrossRef]
84. Feng, B.; Wu, Y.; Ren, Y.; Chen, Y.; Yuan, K.; Deng, Y.; Wei, J. Self-template synthesis of mesoporous Au-SnO₂ nanospheres for low-temperature detection of triethylamine vapor. *Sens. Actuators B Chem.* **2022**, *356*, 131358. [CrossRef]
85. Sun, H.; Tang, X.; Zhang, J.; Li, S.; Liu, L. MOF-derived bow-like Ga-doped Co₃O₄ hierarchical architectures for enhanced triethylamine sensing performance. *Sens. Actuators B Chem.* **2021**, *346*, 130546. [CrossRef]
86. Zhao, Q.; Zhuang, G.; Zhao, Y.; Yang, L.; Zhao, J. Y-doped In₂O₃ hollow nanocubes for improved triethylamine-sensing performance. *New J. Chem.* **2021**, *45*, 6773–6779. [CrossRef]
87. Liu, J.; Zhang, L.; Fan, J.; Zhu, B.; Yu, J. Triethylamine gas sensor based on Pt-functionalized hierarchical ZnO microspheres. *Sens. Actuators B Chem.* **2021**, *331*, 129425. [CrossRef]
88. Zhu, M.; Yang, T.; Zhai, C.; Du, L.; Zhang, J.; Zhang, M. Fast triethylamine gas sensing response properties of Ho-doped SnO₂ nanoparticles. *J. Alloys Compd.* **2020**, *817*, 152724. [CrossRef]
89. Zhang, K.; Xie, K.; Maruf Ahmed, M.; Chai, Z.; Zhao, R.; Li, J.; Du, J. Cr-doped SnO₂ microrods adhering nanoparticles for enhanced triethylamine sensing performance. *Mater. Lett.* **2022**, *312*, 131684. [CrossRef]
90. Bi, W.; Wang, W.; Liu, S. Synthesis of Rh-SnO₂ nanosheets and ultra-high triethylamine sensing performance. *J. Alloys Compd.* **2020**, *817*, 152730. [CrossRef]
91. Yu, Y.; Liao, Z.; Meng, F.; Yuan, Z. Theoretical and Experimental Research on Ammonia Sensing Properties of Sulfur-Doped Graphene Oxide. *Chemosensors* **2021**, *9*, 220. [CrossRef]
92. Wang, X.; Han, W.; Yang, J.; Cheng, P.; Wang, Y.; Feng, C.; Wang, C.; Zhang, H.; Sun, Y.; Lu, G. Conductometric ppb-level triethylamine sensor based on macroporous WO₃-W₁₈O₄₉ heterostructures functionalized with carbon layers and PdO nanoparticles. *Sens. Actuators B Chem.* **2022**, *361*, 131707. [CrossRef]
93. Peng, R.; Li, Y.; Liu, T.; Si, P.; Feng, J.; Suhr, J.; Ci, L. Boron-doped graphene coated Au@SnO₂ for high-performance triethylamine gas detection. *Mater. Chem. Phys.* **2020**, *239*, 121961. [CrossRef]
94. Zhang, M.; Zhao, Z.; Hui, B.; Sun, J.; Sun, J.; Tian, W.; Zhang, Z.; Zhang, K.; Xia, Y. Carbonized polymer dots activated hierarchical tungsten oxide for efficient and stable triethylamine sensor. *J. Hazard. Mater.* **2021**, *416*, 126161. [CrossRef]
95. Gai, L.-Y.; Lai, R.-P.; Dong, X.-H.; Wu, X.; Luan, Q.-T.; Wang, J.; Lin, H.-F.; Ding, W.-H.; Wu, G.-L.; Xie, W.-F. Recent advances in ethanol gas sensors based on metal oxide semiconductor heterojunctions. *Rare Met.* **2022**, *41*, 1818–1842. [CrossRef]
96. Liu, Y.; Xiao, S.; Du, K. Chemiresistive Gas Sensors Based on Hollow Heterojunction: A Review. *Adv. Mater. Interfaces* **2021**, *8*, 2002122. [CrossRef]
97. Chen, S.; Gao, N.; Bunes, B.R.; Zang, L. Tunable nanofibril heterojunctions for controlling interfacial charge transfer in chemiresistive gas sensors. *J. Mater. Chem. C* **2019**, *7*, 13709–13735. [CrossRef]
98. Lin, Y.; Fan, Z. Compositing strategies to enhance the performance of chemiresistive CO₂ gas sensors. *Mater. Sci. Semicond. Process.* **2020**, *107*, 104820. [CrossRef]

99. Xu, X.; Liu, W.; Chen, Y.; Wang, S.; Wang, X.; Jiang, H.; Ma, S.; Yuan, F.; Zhang, Q. n-n Heterogeneous MoS₂/SnO₂ Nanotubes and The Excellent Triethylamine (TEA) Sensing Performances. *Mater. Lett.* **2022**, *311*, 131522. [[CrossRef](#)]
100. Xu, H.; Ju, J.; Li, W.; Zhang, J.; Wang, J.; Cao, B. Superior triethylamine-sensing properties based on TiO₂/SnO₂ n-n heterojunction nanosheets directly grown on ceramic tubes. *Sens. Actuators B Chem.* **2016**, *228*, 634–642. [[CrossRef](#)]
101. Xue, D.; Wang, Y.; Cao, J.; Zhang, Z. Hydrothermal Synthesis of CeO₂-SnO₂ Nanoflowers for Improving Triethylamine Gas Sensing Property. *Nanomaterials* **2018**, *8*, 1025. [[CrossRef](#)] [[PubMed](#)]
102. Yang, B.; Myung, N.V.; Tran, T.T. 1D Metal Oxide Semiconductor Materials for Chemiresistive Gas Sensors: A Review. *Adv. Electron. Mater.* **2021**, *7*, 2100271. [[CrossRef](#)]
103. Gao, H.; Ma, Y.; Song, P.; Yang, Z.; Wang, Q. Three-dimensional reduced graphene oxide/cobaltosic oxide as a high-response sensor for triethylamine gas at room temperature. *Mater. Sci. Semicond. Process.* **2021**, *133*, 105904. [[CrossRef](#)]
104. Wang, D.; Gu, K.; Zhang, J.; Xing, D.; Zhang, M. MOF-derived NiWO₄@NiO p-p heterostructure for distinguish detection of TEA and xylene by temperature regulation. *J. Alloys Compd.* **2021**, *875*, 160015. [[CrossRef](#)]
105. Yang, S.; Lei, G.; Xu, H.; Lan, Z.; Wang, Z.; Gu, H. Metal Oxide Based Heterojunctions for Gas Sensors: A Review. *Nanomaterials* **2021**, *11*, 1026. [[CrossRef](#)]
106. Shang, Y.; Shi, W.; Zhao, R.; Ahmed, M.M.; Li, J.; Du, J. Simple self-assembly of 3D laminated CuO/SnO₂ hybrid for the detection of triethylamine. *Chin. Chem. Lett.* **2020**, *31*, 2055–2058. [[CrossRef](#)]
107. Zeng, J.; Rong, Q.; Xiao, B.; Zi, B.; Kuang, X.; Deng, X.; Ma, Y.; Song, Z.; Zhang, G.; Zhang, J.; et al. Ultrasensitive ppb-level trimethylamine gas sensor based on p-n heterojunction of Co₃O₄/WO₃. *Nanotechnology* **2021**, *32*, 505511. [[CrossRef](#)]
108. Yu, Q.; Jin, R.; Zhao, L.; Wang, T.; Liu, F.; Yan, X.; Wang, C.; Sun, P.; Lu, G. MOF-Derived Mesoporous and Hierarchical Hollow-Structured In₂O₃-NiO Composites for Enhanced Triethylamine Sensing. *ACS Sens.* **2021**, *6*, 3451–3461. [[CrossRef](#)]
109. Bai, S.; Tian, Y.; Sun, J.; Tong, Z.; Luo, R.; Li, D.; Chen, A. Heterostructures of polyaniline@SnO₂ loading on flexible PET thin films for triethylamine detection at room temperature. *New J. Chem.* **2016**, *40*, 4595–4600. [[CrossRef](#)]
110. Galstyan, V. “Quantum dots: Perspectives in next-generation chemical gas sensors” A review. *Anal. Chim. Acta* **2021**, *1152*, 238192. [[CrossRef](#)]
111. Liu, J.; Zhu, B.; Zhang, L.; Fan, J.; Yu, J. 0D/2D CdS/ZnO composite with n-n heterojunction for efficient detection of triethylamine. *J. Colloid Interface Sci.* **2021**, *600*, 898–909. [[CrossRef](#)] [[PubMed](#)]
112. Liu, J.; Peng, Y.; Zhu, B.; Li, Y.; Zhang, L.; Yu, J. ZIF-8 derived ZnO-CsPbBr₃ polyhedrons for efficient triethylamine detection. *Sens. Actuators B Chem.* **2022**, *357*, 131366. [[CrossRef](#)]
113. Meng, F.; Zheng, H.; Chang, Y.; Zhao, Y.; Li, M.; Wang, C.; Sun, Y.; Liu, J. One-Step Synthesis of Au/SnO₂/RGO Nanocomposites and Their VOC Sensing Properties. *IEEE Trans. Nanotechnol.* **2018**, *17*, 212–219. [[CrossRef](#)]
114. Meng, F.; Li, X.; Yuan, Z.; Lei, Y.; Qi, T.; Li, J. Ppb-Level Xylene Gas Sensors Based on Co₃O₄ Nanoparticle-Coated Reduced Graphene Oxide(rGO) Nanosheets Operating at Low Temperature. *IEEE Trans. Instrum. Meas.* **2021**, *70*, 1–10. [[CrossRef](#)]
115. Xiao, Z.; Kong, L.B.; Ruan, S.; Li, X.; Yu, S.; Li, X.; Jiang, Y.; Yao, Z.; Ye, S.; Wang, C.; et al. Recent development in nanocarbon materials for gas sensor applications. *Sens. Actuators B Chem.* **2018**, *274*, 235–267. [[CrossRef](#)]
116. Bag, A.; Lee, N.-E. Gas sensing with heterostructures based on two-dimensional nanostructured materials: A review. *J. Mater. Chem. C* **2019**, *7*, 13367–13383. [[CrossRef](#)]
117. Liu, B.; Zhu, Q.; Pan, Y.; Huang, F.; Tang, L.; Liu, C.; Cheng, Z.; Wang, P.; Ma, J.; Ding, M. Single-Atom Tailoring of Two-Dimensional Atomic Crystals Enables Highly Efficient Detection and Pattern Recognition of Chemical Vapors. *ACS Sens.* **2022**, *7*, 1533–1543. [[CrossRef](#)]
118. Huang, X.; Qi, X.; Boey, F.; Zhang, H. Graphene-based composites. *Chem. Soc. Rev.* **2012**, *41*, 666–686. [[CrossRef](#)]
119. Kumar, Y.R.; Deshmukh, K.; Sadasivuni, K.K.; Pasha, S.K.K. Graphene quantum dot based materials for sensing, bio-imaging and energy storage applications: A review. *RSC Adv.* **2020**, *10*, 23861–23898. [[CrossRef](#)]
120. Chu, X.; Zhu, X.; Dong, Y.; Zhang, W.; Bai, L. Formaldehyde Sensing Properties of SnO–Graphene Composites Prepared via Hydrothermal Method. *J. Mater. Sci. Technol.* **2015**, *31*, 913–917. [[CrossRef](#)]
121. Wang, T.; Huang, D.; Yang, Z.; Xu, S.; He, G.; Li, X.; Hu, N.; Yin, G.; He, D.; Zhang, L. A Review on Graphene-Based Gas/Vapor Sensors with Unique Properties and Potential Applications. *Nanomicro Lett.* **2016**, *8*, 95–119. [[CrossRef](#)] [[PubMed](#)]
122. Bai, S.; Sun, L.; Sun, J.; Han, J.; Zhang, K.; Li, Q.; Luo, R.; Li, D.; Chen, A. Pine dendritic bismuth vanadate loaded on reduced graphene oxide for detection of low concentration triethylamine. *J. Colloid Interface Sci.* **2021**, *587*, 183–191. [[CrossRef](#)] [[PubMed](#)]
123. Wei, Q.; Sun, J.; Song, P.; Li, J.; Yang, Z.; Wang, Q. MOF-derived α -Fe₂O₃ porous spindle combined with reduced graphene oxide for improvement of TEA sensing performance. *Sens. Actuators B Chem.* **2020**, *304*, 127306. [[CrossRef](#)]
124. Yu, T.; Li, X.; Chen, B.; Yang, Y.; Xu, K.; Liu, Y.; Gong, W.; Yuan, C.; Yang, Y. Enhanced Gas Sensing Performance of rGO Wrapped Crystal Facet-Controlled Co₃O₄ Nanocomposite Heterostructures. *J. Phys. Chem. C* **2022**, *126*, 4879–4888. [[CrossRef](#)]
125. Naguib, M.; Kurtoglu, M.; Presser, V.; Lu, J.; Niu, J.; Heon, M.; Hultman, L.; Gogotsi, Y.; Barsoum, M.W. Two-dimensional nanocrystals produced by exfoliation of Ti₃AlC₂. *Adv. Mater.* **2011**, *23*, 4248–4253. [[CrossRef](#)]
126. Mehdi Aghaei, S.; Aasi, A.; Panchapakesan, B. Experimental and Theoretical Advances in MXene-Based Gas Sensors. *ACS Omega* **2021**, *6*, 2450–2461. [[CrossRef](#)]
127. Bhardwaj, R.; Hazra, A. MXene-based gas sensors. *J. Mater. Chem. C* **2021**, *9*, 15735–15754. [[CrossRef](#)]
128. Khazaei, M.; Mishra, A.; Venkataramanan, N.S.; Singh, A.K.; Yunoki, S. Recent advances in MXenes: From fundamentals to applications. *Curr. Opin. Solid State Mater. Sci.* **2019**, *23*, 164–178. [[CrossRef](#)]

129. He, T.; Liu, W.; Lv, T.; Ma, M.; Liu, Z.; Vasiliev, A.; Li, X. MXene/SnO₂ heterojunction based chemical gas sensors. *Sens. Actuators B Chem.* **2021**, *329*, 129275. [[CrossRef](#)]
130. Tian, X.; Yao, L.; Cui, X.; Zhao, R.; Chen, T.; Xiao, X.; Wang, Y. A two-dimensional Ti₃C₂T_x MXene@TiO₂/MoS₂ heterostructure with excellent selectivity for the room temperature detection of ammonia. *J. Mater. Chem. A* **2022**, *10*, 5505–5519. [[CrossRef](#)]
131. Liang, D.; Song, P.; Liu, M.; Wang, Q. 2D/2D SnO₂ nanosheets/Ti₃C₂T_x MXene nanocomposites for detection of triethylamine at low temperature. *Ceram. Int.* **2022**, *48*, 9059–9066. [[CrossRef](#)]
132. Anichini, C.; Czepa, W.; Pakulski, D.; Aliprandi, A.; Ciesielski, A.; Samori, P. Chemical sensing with 2D materials. *Chem. Soc. Rev.* **2018**, *47*, 4860–4908. [[CrossRef](#)] [[PubMed](#)]
133. Ping, J.; Fan, Z.; Sindoro, M.; Ying, Y.; Zhang, H. Recent Advances in Sensing Applications of Two-Dimensional Transition Metal Dichalcogenide Nanosheets and Their Composites. *Adv. Funct. Mater.* **2017**, *27*, 1605817. [[CrossRef](#)]
134. Joshi, N.; Hayasaka, T.; Liu, Y.; Liu, H.; Oliveira, O.N., Jr.; Lin, L. A review on chemiresistive room temperature gas sensors based on metal oxide nanostructures, graphene and 2D transition metal dichalcogenides. *Mikrochim. Acta* **2018**, *185*, 213. [[CrossRef](#)]
135. Xu, X.L.; Wang, X.P.; Chen, Y.; Liu, W.W.; Wang, S.Y.; Yuan, F.Q.; Ma, S.Y. Design of MoS₂/ZnO bridge-like hetero-nanostructures to boost triethylamine (TEA) sensing. *Vacuum* **2022**, *196*, 110733. [[CrossRef](#)]
136. Hou, X.; Wang, Z.; Fan, G.; Ji, H.; Yi, S.; Li, T.; Wang, Y.; Zhang, Z.; Yuan, L.; Zhang, R.; et al. Hierarchical three-dimensional MoS₂/GO hybrid nanostructures for triethylamine-sensing applications with high sensitivity and selectivity. *Sens. Actuators B Chem.* **2020**, *317*, 128236. [[CrossRef](#)]
137. Shellaiah, M.; Sun, K.W. Review on Sensing Applications of Perovskite Nanomaterials. *Chemosensors* **2020**, *8*, 55. [[CrossRef](#)]
138. Qin, W.; Yuan, Z.; Gao, H.; Zhang, R.; Meng, F. Perovskite-structured LaCoO₃ modified ZnO gas sensor and investigation on its gas sensing mechanism by first principle. *Sens. Actuators B Chem.* **2021**, *341*, 130015. [[CrossRef](#)]
139. Bulemo, P.M.; Kim, I.-D. Recent advances in ABO₃ perovskites: Their gas-sensing performance as resistive-type gas sensors. *J. Korean Ceram. Soc.* **2019**, *57*, 24–39. [[CrossRef](#)]
140. Qin, W.; Yuan, Z.; Shen, Y.; Zhang, R.; Meng, F. Phosphorus-doped porous perovskite LaFe_{1-x}P_xO_{3-δ} nanosheets with rich surface oxygen vacancies for ppb level acetone sensing at low temperature. *Chem. Eng. J.* **2022**, *431*, 134280. [[CrossRef](#)]
141. Yan, Y.; Liu, J.; Zhang, H.; Song, D.; Li, J.; Yang, P.; Zhang, M.; Wang, J. One-pot synthesis of cubic ZnSnO₃/ZnO heterostructure composite and enhanced gas-sensing performance. *J. Alloys Compd.* **2019**, *780*, 193–201. [[CrossRef](#)]
142. Chu, X.; Zhou, S.; Zhang, W.; Shui, H. Trimethylamine sensing properties of nano-LaFeO₃ prepared using solid-state reaction in the presence of PEG400. *Mater. Sci. Eng. B* **2009**, *164*, 65–69. [[CrossRef](#)]
143. Zheng, L.; Zhao, Y.; Xu, Y.; Yang, C.; Zhang, J.; Liu, X. Susceptible CoSnO₃ nanoboxes with p-type response for triethylamine detection at low temperature. *CrystEngComm* **2020**, *22*, 2795–2805. [[CrossRef](#)]
144. Hao, P.; Lin, Z.; Song, P.; Yang, Z.; Wang, Q. rGO-wrapped porous LaFeO₃ microspheres for high-performance triethylamine gas sensors. *Ceram. Int.* **2020**, *46*, 9363–9369. [[CrossRef](#)]
145. Liu, M.; Wang, C.; Yang, M.; Tang, L.; Wang, Q.; Sun, Y.; Xu, Y. Novel strategy to construct porous Sn-doped ZnO/ZnFe₂O₄ heterostructures for superior triethylamine detection. *Mater. Sci. Semicond. Process.* **2021**, *125*, 105643. [[CrossRef](#)]
146. Liu, F.; Chu, X.; Dong, Y.; Zhang, W.; Sun, W.; Shen, L. Acetone gas sensors based on graphene-ZnFe₂O₄ composite prepared by solvothermal method. *Sens. Actuators B Chem.* **2013**, *188*, 469–474. [[CrossRef](#)]
147. Fergus, J.W. Perovskite oxides for semiconductor-based gas sensors. *Sens. Actuators B Chem.* **2007**, *123*, 1169–1179. [[CrossRef](#)]
148. Li, Y.; Yuan, Z.; Meng, F. Spinel-Type Materials Used for Gas Sensing: A Review. *Sensors* **2020**, *20*, 5413. [[CrossRef](#)] [[PubMed](#)]
149. Tian, K.; Zhang, W.; Sun, S.-N.; Xing, L.; Li, Z.-Y.; Zhang, T.-T.; Yang, N.-N.; Kuang, B.-B.; Li, H.-Y. Design and fabrication of spinel nanocomposites derived from perovskite hydroxides as gas sensing layer for volatile organic compounds detection. *Sens. Actuators B Chem.* **2021**, *329*, 129076. [[CrossRef](#)]
150. Ma, P.; Li, X.; Zhang, Y.; Han, L.; Xu, Y. Hierarchical spinel-type corn-like MGa₂O₄ (M = Ni, Co) architectures for selective triethylamine gas sensors. *Mater. Sci. Semicond. Process.* **2021**, *133*, 105993. [[CrossRef](#)]
151. Yang, C.; Xu, Y.; Zheng, L.; Zhao, Y.; Zheng, W.; Liu, X.; Zhang, J. Hierarchical NiCo₂O₄ microspheres assembled by nanorods with p-type response for detection of triethylamine. *Chin. Chem. Lett.* **2020**, *31*, 2077–2082. [[CrossRef](#)]
152. Xu, X.; Wang, S.; Liu, W.; Chen, Y.; Ma, S.; Yun, P. An excellent triethylamine (TEA) sensor based on unique hierarchical MoS₂/ZnO composites composed of porous microspheres and nanosheets. *Sens. Actuators B Chem.* **2021**, *333*, 129616. [[CrossRef](#)]
153. Zhao, Y.; Yuan, X.; Sun, Y.; Wang, Q.; Xia, X.-Y.; Tang, B. Facile synthesis of tortoise shell-like porous NiCo₂O₄ nanoplate with promising triethylamine gas sensing properties. *Sens. Actuators B Chem.* **2020**, *323*, 128663. [[CrossRef](#)]
154. Ebrahimifard, R.; Abdizadeh, H.; Golobostanfard, M.R. Controlling the extremely preferred orientation texturing of sol-gel derived ZnO thin films with sol and heat treatment parameters. *J. Sol-Gel Sci. Technol.* **2019**, *93*, 28–35. [[CrossRef](#)]
155. Lou, C.; Li, Z.; Yang, C.; Liu, X.; Zheng, W.; Zhang, J. Rational design of ordered porous SnO₂/ZrO₂ thin films for fast and selective triethylamine detection with humidity resistance. *Sens. Actuators B Chem.* **2021**, *333*, 129572. [[CrossRef](#)]
156. Yu, H.; Xu, H.; Li, W.; Zhai, T.; Chen, Z.; Wang, J.; Cao, B. Enhanced triethylamine sensing properties by designing Au@SnO₂/ZnO nanosheets directly on alumina tubes. *Surf. Interfaces* **2018**, *10*, 85–92. [[CrossRef](#)]
157. Xie, G.; Cheng, G.; Zhu, D.; Yan, J.; Ma, J.; Lv, T.; Zhang, J.; Han, W.; Long, Y.Z. Progress of superconducting nanofibers via electrospinning. *J. Phys. Condens. Matter.* **2021**, *34*, 043002. [[CrossRef](#)]
158. Li, Z.; Liu, X.; Zhou, M.; Zhang, S.; Cao, S.; Lei, G.; Lou, C.; Zhang, J. Plasma-induced oxygen vacancies enabled ultrathin ZnO films for highly sensitive detection of triethylamine. *J. Hazard. Mater.* **2021**, *415*, 125757. [[CrossRef](#)]

159. Mostafa, A.M. The enhancement of nonlinear absorption of Zn/ZnO thin film by creation oxygen vacancies via infrared laser irradiation and coating with Ag thin film via pulsed laser deposition. *J. Mol. Struct.* **2021**, *1226*, 129407. [[CrossRef](#)]
160. Song, X.; Li, L.; Chen, X.; Xu, Q.; Song, B.; Pan, Z.; Liu, Y.; Juan, F.; Xu, F.; Cao, B. Enhanced triethylamine sensing performance of α -Fe₂O₃ nanoparticle/ZnO nanorod heterostructures. *Sens. Actuators B Chem.* **2019**, *298*, 126917. [[CrossRef](#)]
161. Yoon, J.; Kim, J.; Park, S.; Jeong, Y.W.; Lee, C.; Oh, S.G. Fabrication of Ag-doped ZnO/PAN composite nanofibers by electrospinning: Photocatalytic and antiviral activities. *Korean J. Chem. Eng.* **2022**, *39*, 1632–1640. [[CrossRef](#)]
162. Lee, J.; Lee, K.J. Colloid Syringeless Electrospinning toward Nonwoven Nanofiber Web Containing a Massive Amount of Inorganic Fillers. *Macromol. Mater. Eng.* **2022**, *307*, 2100818. [[CrossRef](#)]
163. Ma, Q.; Li, H.; Chu, S.; Liu, Y.; Liu, M.; Fu, X.; Li, H.; Guo, J. In₂O₃ Hierarchical Structures of One-Dimensional Electrospun Fibers with in Situ Growth of Octahedron-like Particles with Superior Sensitivity for Triethylamine at Near Room Temperature. *ACS Sustain. Chem. Eng.* **2020**, *8*, 5240–5250. [[CrossRef](#)]
164. Wang, X.-X.; Wang, N.; Qiu, H.; Song, W.; Liu, Q.; Fan, Z.; Yu, M.; Ramakrishna, S.; Long, Y.-Z. Anisotropic nanogenerator for anticounterfeiting and information encrypted transmission. *Nano Energy* **2020**, *71*, 104572. [[CrossRef](#)]
165. Xu, D.; Chen, Y.; Qiu, T.; Qi, S.; Zhang, L.; Yin, M.; Ge, K.; Wei, X.; Tian, X.; Wang, P.; et al. Hierarchical mesoporous SnO₂ nanotube templated by staphylococcus aureus through electrospinning for highly sensitive detection of triethylamine. *Mater. Sci. Semicond. Process.* **2021**, *136*, 106129. [[CrossRef](#)]
166. Cheng, Y.; Ren, B.; Xu, K.; Jeerapan, I.; Chen, H.; Li, Z.; Ou, J.Z. Recent progress in intrinsic and stimulated room-temperature gas sensors enabled by low-dimensional materials. *J. Mater. Chem. C* **2021**, *9*, 3026–3051. [[CrossRef](#)]
167. Sudha, S.; Ramprasad, R.; Cholan, S.; Gokul, B.; Sridhar, S.; Elhosiny Ali, H.; Shkir, M. Enhanced triethylamine gas sensing and photocatalytic performance of Sn doped NiO (SNO) nanoparticles. *Inorg. Chem. Commun.* **2022**, *136*, 109104. [[CrossRef](#)]
168. Liu, S.-R.; Guan, M.-Y.; Li, X.-Z.; Guo, Y. Light irradiation enhanced triethylamine gas sensing materials based on ZnO/ZnFe₂O₄ composites. *Sens. Actuators B Chem.* **2016**, *236*, 350–357. [[CrossRef](#)]
169. Shanmugam, P.; Pushparaj, K.; Sundaramurthy, A.; Sivalingam, Y. Investigation of UV light enhanced gas adsorption properties of CeO₂ Nanoparticles by Scanning Kelvin Probe system. *J. Mol. Struct.* **2022**, *1250*, 131831. [[CrossRef](#)]
170. Yang, T.; Gu, K.; Zhu, M.; Lu, Q.; Zhai, C.; Zhao, Q.; Yang, X.; Zhang, M. ZnO-SnO₂ heterojunction nanobelts: Synthesis and ultraviolet light irradiation to improve the triethylamine sensing properties. *Sens. Actuators B Chem.* **2019**, *279*, 410–417. [[CrossRef](#)]